

1 **Heterogeneous Interactions between SO₂ and**
2 **Organic Peroxides in Submicron Aerosol**

3
4 Shun Yao Wang¹, Tengyu Liu², Jinmyung Jang¹,
5 Jonathan P.D. Abbatt² and Arthur W.H. Chan^{1*}
6
7
8
9

10 ¹Department of Chemical Engineering and Applied Chemistry, University of Toronto,
11 Toronto, Ontario, M5S 3E5, Canada

12 ²Department of Chemistry, University of Toronto, Toronto, Ontario, M5S 3H6, Canada
13
14
15
16
17
18
19
20

21 **Correspondence to:* Arthur W.H. Chan (arthurwh.chan@utoronto.ca)

22 **Abstract**

23 Atmospheric models often underestimate particulate sulfate, a major component in ambient
24 aerosol, suggesting missing sulfate formation mechanisms in the models. Heterogeneous
25 reactions between SO₂ and aerosol play an important role in particulate sulfate formation and its
26 physicochemical evolution. Here we study the reactive uptake kinetics of SO₂ onto aerosol
27 containing organic peroxides. We present chamber studies of SO₂ reactive uptake performed
28 under different relative humidities (RH), particulate peroxide contents, peroxide types, and
29 aerosol acidities. Using different model organic peroxides mixed with ammonium sulfate
30 particles, SO₂ uptake coefficient (γ_{SO_2}) was found to be exponentially dependent on RH. γ_{SO_2}
31 increases from 10⁻³ at RH 25 % to 10⁻² at RH 71 % as measured for an organic peroxide with
32 multiple O-O groups. Under similar conditions, the kinetics in this study were found to be
33 structurally dependent: organic peroxides with multiple peroxide groups have a higher γ_{SO_2} than
34 those with only one peroxide group, consistent with the reactivity trend observed previously in
35 the aqueous phase. In addition, γ_{SO_2} is linearly related to particle-phase peroxide content, which
36 in turn depends on gas-particle partitioning of organic peroxides. Aerosol acidity plays a
37 complex role in determining SO₂ uptake rate, influenced by the effective Henry's Law constant
38 of SO₂ and the condensed phase kinetics of the peroxide-SO₂ reaction in the highly concentrated
39 aerosol phase. These uptake coefficients are consistently higher than those calculated from the
40 reaction kinetics in the bulk aqueous phase, and we show experimental evidence suggesting that
41 other factors, such as particle-phase ionic strength, can play an essential role in determining the
42 uptake kinetics. γ_{SO_2} for different types of secondary organic aerosol (SOA) were measured to be
43 on the order of 10⁻⁴. Overall, this study provides quantitative evidence of the multiphase

44 reactions between SO₂ and organic peroxides, highlighting the important factors that govern the
45 uptake kinetics.

46 **Introduction**

47 Sulfate and organic compounds are ubiquitous particulate components in both polluted and
48 pristine environments (Chen et al., 2009;Andreae et al., 2018;He et al., 2011;Sun et al.,
49 2013;Huang et al., 2014), with important implications for public health and global climate
50 (Hallquist et al., 2009). Particulate sulfate can form via S(IV) oxidation by OH radicals in the gas
51 phase and via oxidation in cloud water, fog droplets or the aerosol aqueous phase, including by
52 H₂O₂, O₂ (catalyzed by transition metals), O₃, NO₂ and small organic peroxides (methyl
53 hydroperoxide and peroxyacetic acid) (Seinfeld and Pandis, 2012). However, atmospheric
54 models tend to underestimate particulate sulfate production on both global (Tie et al., 2001;Yang
55 et al., 2017;Fairlie et al., 2010) and regional scales, especially during heavy haze episodes (Wang
56 et al., 2014;Zheng et al., 2015;Sha et al., 2019;Gao et al., 2016;Li et al., 2017;Huang et al.,
57 2019), suggesting that the overall kinetics may be underestimated and/or important mechanisms
58 may be missing in models.

59 To reconcile these differences, studies have investigated novel reaction mechanisms of sulfate
60 formation. Stabilized Criegee intermediates (sCIs) were hypothesized to oxidize SO₂ rapidly and
61 potentially serve as an important source of ambient sulfate (Mauldin et al., 2012). In the work by
62 Newland et al. (2015) and Nguyen et al. (2016), this sCI pathway was shown to play a minor role
63 in sulfate formation. More recently, when Liu et al. (2019) applied this mechanism and kinetics
64 to a source-oriented WRF-Chem model, the sCIs pathway was found to only account for at most
65 9 % of the total particulate sulfate. Reactive nitrogen species (such as NO₂) have also been
66 proposed as a dominant sulfate formation pathway when aerosol pH was estimated to be 5-6 in

67 Cheng et al. (2016) and close to 7 in Wang et al. (2016) under severe haze scenarios. While such
68 high aerosol pH is not substantiated by some thermodynamic modeling results, which concluded
69 that pH ranges between 4 and 5 in polluted regions (Song et al., 2018;Guo et al., 2017), other
70 studies that highlighted the roles of ammonia and dust found aerosol pH could be higher than 6
71 (Shi et al., 2017; Ding et al., 2019). Furthermore, higher aerosol water content and PM mass
72 concentration in polluted areas have been shown to enhance aerosol pH via a multiphase
73 buffering process (Zheng et al., 2020). Meanwhile, a recent modeling study incorporating this
74 heterogeneous NO_x mechanism still exhibited a discrepancy of 20 % between the predicted and
75 observed sulfate, indicating the possibility of unknown mechanisms (Huang et al., 2019). Other
76 factors may play a role in enhancing the particle-phase sulfate formation rates. Chen et al. (2019)
77 investigated the synergistic effects of NO_2 and NH_3 on sulfate formation, and found that the rate
78 of this reaction can be enhanced by the high ionic strength in the particle phase. This
79 enhancement effect by solute strength on sulfate formation was also investigated for the H_2O_2
80 pathway in aerosol liquid water. Liu et al. (2020) found ionic strength and general acid-catalyzed
81 mechanisms can cause the S(VI) formation rate to be nearly 50 times faster in aerosol phase than
82 in dilute solutions. On the other hand, during the severe haze episodes in China (Li et al., 2020;
83 Guo et al., 2017), transition metal ion (TMI) catalysis of SO_2 oxidation by O_2 can be
84 significantly suppressed in the aerosol phase due to high ionic strength (Liu et al., 2020;Cheng et
85 al., 2016; Su et al., 2020).

86 In addition to high solute strength, submicron aerosol is also rich in organic compounds (Jimenez
87 et al., 2009;Hallquist et al., 2009). In recent years, many studies have investigated the potential
88 role of heterogeneous interactions between SO_2 and organic aerosol on particulate sulfate
89 formation. Song et al. (2019) found heterogeneous oxidation of hydroxymethanesulfonate

90 (HMS) by OH can trigger rapid sulfate formation. Wang et al. (2020) studied photosensitizers in
91 ambient particles and found this pathway could be essential under specific light conditions.
92 Recent studies found reactive intermediates from isoprene oxidation (Huang et al., 2019) and
93 benzoic acid (Huang et al., 2020), can yield a variety of organosulfur species upon catalysis by
94 TMI. Other studies have also investigated the interactions between secondary organic aerosol
95 (SOA) and SO₂. Field observations found that ambient sulfate abundance is highly correlated
96 with SOA formation (Yee et al., 2020; Xu et al., 2015). Liu et al. (2019) found that SO₂ enhances
97 SOA formation and average carbon oxidation state during methoxyphenol photooxidation. By
98 performing chamber experiments with limonene SOA formation in the presence of SO₂, Ye et al.
99 (2018) also observed significant SO₂ decay along with increased SOA yields and carbon
100 oxidation state, proposing that organic peroxides in SOA may be the key reactive intermediates
101 for SO₂ oxidation.

102 Organic peroxides are key intermediates for aerosol formation and ubiquitously exist in many
103 SOA systems (Hallquist et al., 2009; Bianchi et al., 2019). Numerous studies have reported
104 peroxide content of 20-60 % for isoprene and monoterpene derived SOA (Surratt et al., 2006; Ng
105 et al., 2008; Ye et al., 2018; Epstein et al., 2014). A significant fraction of organic peroxide
106 (30 %- 50%) has also been found in naphthalene-derived SOA under low/high NO_x conditions
107 (Kautzman et al., 2009). Using model simulations, Bonn et al. (2004) found organic
108 hydroperoxides can account for up to 60 % of global SOA. The aqueous phase reaction kinetics
109 between organic peroxides and dissolved SO₂ have been explored in previous studies (Lind et al.,
110 1987; Gunz and Hoffmann, 1990; Wang et al., 2019; Dovrou et al., 2019; Yao et al., 2019). The
111 second order reaction rate constants for organic peroxides in SOA (Dovrou et al., 2019; Yao et
112 al., 2019) and S(IV) were measured to be on the order of 10²-10³ M⁻¹ s⁻¹, which are within the

113 range of those measured for commercially available organic peroxides (Wang et al., 2019) and
114 small organic peroxides (Lind et al., 1987). Yao et al. (2019) quantified the reactive uptake
115 coefficient of SO₂ (γ_{SO_2}) onto α -pinene SOA to be on the order of 10⁻⁴-10⁻³, which is positively
116 dependent on RH and inferred particle-phase peroxide content. These reactions are also linked to
117 the formation of organosulfates (Wang et al., 2019). Both inorganic sulfate (85-90 %) and
118 organosulfates (10-15 %) were observed as products of SO₂ reactive uptake onto SOA (Yao et
119 al., 2019).

120 Given the potential significance of SO₂ reactive uptake in particulate sulfate formation, a more
121 in-depth study is needed to determine the important factors that govern the heterogeneous
122 kinetics of SO₂ onto organic peroxide containing aerosol. In this study, we measured γ_{SO_2} for two
123 categories of aerosol: 1. Model organic peroxides mixed with ammonium sulfate or malonic acid
124 and 2. SOA from a few representative biogenic and anthropogenic precursors. The impacts of
125 RH, peroxide type, peroxide content, and condensed phase pH on SO₂ reactive uptake were
126 evaluated systematically with the goal of better understanding atmospheric multiphase sulfate
127 formation.

128

129 **2. Methods**

130 The reactive uptake of SO₂ onto peroxide-containing particles was studied in a 1 m³ Teflon
131 chamber under ambient temperature and pressure. In brief, generated particles and SO₂ were
132 introduced into the chamber separately. The consumption of SO₂, changes in particle size
133 distribution and chemical composition were monitored to estimate the reactive uptake
134 coefficients. Particles were also collected on filters for offline chemical characterization.

135

136 **2.1 Seed aerosol generation**

137 In this work, two types of aerosol were used to investigate the uptake of SO₂. The first is
138 ammonium sulfate or malonic acid mixed with model organic peroxides (Fig. S1). In this first set
139 of experiments, an aerosol atomizer (Model 3076, TSI Inc., USA) was used to generate aqueous
140 particles from dilute solution. Each solution consists of ammonium sulfate ($\geq 99\%$, Sigma-
141 Aldrich) or malonic acid (99%, Sigma-Aldrich) and a model organic peroxide in ultrapure water
142 (HPLC grade, Fisher Chemical). For the experiments investigating the relationship between γ_{SO_2}
143 and peroxide type (Expt. 2-14, Table S1), different commercially available organic peroxides
144 were used, including tert-butyl hydroperoxide (70 wt. % in water, Sigma-Aldrich), cumene
145 hydroperoxide (80 wt. % in water, Sigma-Aldrich), and 2-butanone peroxide (40% wt. % in
146 water, Sigma-Aldrich). The molar ratio of organic peroxide to ammonium sulfate in the
147 atomizing solution was 2:1 with the aim of being atmospherically relevant (corresponding to
148 maximum particulate peroxide molar fraction of 66% and mass fraction of approximately 50-
149 70% if all the organic peroxides were assumed to remain in the particle phase). This ratio was
150 used as a proxy for total peroxide content in both gas and particle phase relative to that of
151 ammonium sulfate upon atomization. For the experiments studying the relationship between γ_{SO_2}
152 and particle-phase peroxide content, the molar ratio of organic peroxide to ammonium sulfate
153 (Expt. 10-12, 15-18, Table S1) in the solution was adjusted to be 0.02, 0.2, 1, 2, and 4,
154 respectively. In experiments where malonic acid was used (Expt. 19-22, Table S1), molar ratios
155 of 0.2, 1, 2, and 4 were adopted. For measuring γ_{SO_2} with different aerosol pH (Expt. 17, 23-25,
156 Table S1), different amounts of HCl (37%, Sigma-Aldrich) were added into the solution (0,
157 0.00002 M, 0.0001 M, 0.001 M HCl) prior to atomization. The initial pH of aerosol (2.5, 2.2,
158 1.6, 1, respectively) were modeled using E-AIM III model (Clegg et al., 1998) based on the

159 initial molar ratios of inorganic species (H^+ , NH_4^+ , SO_4^{2-} , Cl^-) in the atomizing solution and
160 measured RH (around 50 %). The atomized particles were flowed into the chamber without
161 drying, and therefore assumed to remain deliquesced under the range of RH we studied. Expt. 2-
162 14 (Table S1) also represent those where the relationship between γ_{SO_2} and RH conditions were
163 studied.

164 In the second set of experiments, the uptake of SO_2 onto SOA was investigated (Fig. S2, Expt.
165 26-28, Table S1). A custom-built 10 L quartz oxidation flow reactor was used to produce SOA
166 (Ye et al., 2016) from different hydrocarbon precursors. In this work, we studied SOA formed
167 from toluene photooxidation, limonene ozonolysis and α -pinene ozonolysis, 3 of the most
168 commonly studied SOA systems (Ng et al., 2007; Hildebrandt et al., 2009; Hartz et al.,
169 2005; Varutbangkul et al., 2006). Toluene (analytical standard, Sigma Aldrich) was injected
170 continuously into zero air flow by a syringe (1000 mL, Hamilton) installed on a syringe pump
171 (KDS Legato100) to achieve an initial concentration of 0.5 ppm. Limonene (Sigma-Aldrich,
172 97 %) and α -pinene (Sigma-Aldrich, 98 %) were pre-dissolved in cyclohexane (Sigma-Aldrich,
173 99.5 %) with a volumetric ratio of 1: 1500 and 1: 500 to ensure that OH formed from limonene
174 or α -pinene ozonolysis is scavenged by cyclohexane, estimated based on the rate constants
175 (Atkinson and Arey, 2003). The initial steady-state concentrations of limonene and α -pinene
176 were controlled to be around 2 ppm and 1 ppm entering the flow tube. O_3 , used as the oxidant
177 (for limonene and α -pinene) or the OH precursor (for toluene), was generated by passing 0.5 L
178 min^{-1} pure oxygen (99.6 %, Linde, Mississauga, Canada) through an O_3 generator (no.
179 97006601, UVP, Cambridge, UK). Humidified air was produced by bubbling zero air through a
180 custom-made humidifier at a flow rate of 1 L min^{-1} . The photolysis of O_3 produces $\text{O} (^1\text{D})$,
181 which reacts with water vapour to produce $\cdot\text{OH}$ with illumination from the 254 nm UV lamps

182 (UVP, Cambridge, UK) to initiate the photooxidation of toluene. The average residence time
183 inside the flow tube was controlled to be around 5 minutes. A gas chromatography–flame
184 ionization detector (GC-FID, model 8610C, SRI Instruments Inc., LV, USA) equipped with a
185 Tenax® TA trap was used to monitor the concentration of hydrocarbon precursors at the
186 inlet/outlet of the flow reactor. In all cases, the O₃ concentration was maintained to be at least 10
187 times higher than that of the hydrocarbon. Temperature and relative humidity were monitored by
188 an Omega HX94C RH/T transmitter. Particle size distribution and volume concentration were
189 monitored using a custom-built scanning mobility particle sizer (SMPS), which is a combination
190 of a differential mobility analyzer column (DMA, model 3081, TSI, Shoreview, MN, USA) with
191 flow controls and a condensation particle counter (CPC, model 3772, TSI, Shoreview, MN,
192 USA).

193

194 **2.2 Quantification of γ_{SO_2}**

195 Prior to each experiment, the chamber was flushed by purified air overnight with a flow rate of
196 25 L min⁻¹ until particle number concentration was less than 5 cm⁻³ and SO₂ was less than 1 ppb.
197 To adjust RH, the chamber was humidified by passing purified air through a custom-built
198 humidifier filled with ultra-pure water. For experiments with atomized ammonium sulfate or
199 malonic acid, SO₂ was injected into the chamber prior to the introduction of particles. For
200 experiments studying γ_{SO_2} onto SOA, aerosol generated from the flow tube was injected into the
201 Teflon chamber continuously after passing through an O₃ denuder (Ozone Solutions, Iowa, USA)
202 to achieve specific aerosol concentration inside the chamber prior to SO₂ addition. SO₂ mixing
203 ratio in the chamber during each experiment was continuously monitored using an SO₂ analyzer
204 (Model 43i, Thermo Scientific). The initial mixing ratio of SO₂ in each experiment was

205 controlled to be around 200 ppb. Aerosol size distribution was monitored by SMPS. The reactive
206 uptake coefficient of SO₂ was calculated by integrating the following equation:

$$207 \quad -\frac{d[SO_2]}{dt} = \frac{1}{4}\gamma_{SO_2}A\bar{c}[SO_2] \quad (1)$$

208
209 Where [SO₂] is the SO₂ mixing ratio (ppb) monitored by the SO₂ analyzer; A is the average
210 surface area concentration (μm² cm⁻³) derived from the particle size distribution measured by
211 SMPS; \bar{c} represents the mean molecular velocity (cm s⁻¹) of SO₂. d[SO₂]/dt is solved over the
212 initial SO₂ decay, such that the peroxide concentration in the aerosol liquid phase is assumed to
213 be constant and pseudo-first order kinetics can be applied (Abbatt et al., 2012; Thornton et al.,
214 2003). A summary of all the measured γ_{SO_2} can be found in Table S1. Typical evolution of
215 monitored species can be seen in Fig.1. Control experiments were performed in order to rule out
216 other potential factors (e.g. SO₂ loss in the in-line filter in front of the SO₂ analyzer, interferences
217 inside the SO₂ analyzer, chamber wall losses, SO₂ uptake onto wet ammonium sulfate, gas-phase
218 reaction of SO₂ with peroxide vapour) that may contribute to the SO₂ decay observed during the
219 γ_{SO_2} measurement inside the chamber (Fig. S3-S6). Measurement uncertainty and precision of
220 γ_{SO_2} in this study can be found in Table S1. Also, we observed there was SO₂ repartitioning from
221 the humid chamber wall in the presence of organic peroxide under high RH (Fig. S6b, RH 74 %).
222 The observed SO₂ repartitioning rate was then applied to correct the γ_{SO_2} measured under high
223 RH conditions (above 70 %, Expt.14), and this correction amounts to a 40 % increase in
224 calculated γ_{SO_2} .

225

226 **2.3 Offline peroxide quantification**

227 Aerosol was collected onto 47 mm PTFE (polytetrafluoroethylene) filters with 0.2 μm pore size
228 (Whatman®, GE Healthcare) from the chamber by a diaphragm pump (KNF Neuberger Inc., USA)

229 for offline chemical analysis. The total particulate peroxide content (H₂O₂, ROOH and ROOR) in
 230 these samples prior to SO₂ uptake was quantified using the iodometric–spectrophotometric assay
 231 (Docherty et al., 2005). I₂ produced from the reaction between I⁻ and peroxides can further quickly
 232 combine with the excess amount of I⁻ to form I₃⁻, which has brown color and absorbs UV-vis at
 233 470nm. The SOA extraction was then aliquoted into a 96-well UV plate (Greiner Bio-One,
 234 Kremsmünster, AT) with 160 μL well⁻¹. 20 μL of formic acid (≥ 95 %, Sigma-Aldrich) was added
 235 into each well, following by 20 μL potassium iodide (BioUltra, ≥99.5 %, Sigma-Aldrich) solution
 236 (dissolved in DI water). The plate was then covered by an adhesive plate sealer (EdgeBio,
 237 Gaithersburg, USA) immediately in order to avoid reagent evaporation and O₂ oxidation. After
 238 incubation for an hour in the dark, the UV-vis absorption at 470nm was measured using a UV-vis
 239 spectrophotometer (Spectramax 190, Molecular Devices Corporation, Sunnyvale, CA) and then
 240 converted to peroxide concentration using the calibration curve made by tert-butyl hydroperoxide
 241 (70 wt. % in H₂O, Sigma-Aldrich) with a series of concentrations (0-10mM). An average
 242 molecular mass for seed particles (organics + ammonium sulfate) was assumed based on the
 243 chemical composition in order to calculate the molar fraction of total peroxides using the following
 244 equation:

$$\text{Molar fraction of peroxide} = \frac{N_{\text{peroxide}}}{N_{\text{aerosol}}} = N_{\text{peroxide}} \frac{M_{(NH_4)_2SO_4} f_{(NH_4)_2SO_4} + M_{\text{peroxide}} f_{\text{peroxide}}}{m_{\text{aerosol}}} \quad (2)$$

247 where m_{aerosol} is the weighed aerosol mass on the filter; $M_{(NH_4)_2SO_4}$ and M_{peroxide} are the
 248 molecular mass of ammonium sulfate and peroxide, respectively; $f_{(NH_4)_2SO_4}$ and f_{peroxide} are the
 249 initial molar fraction of ammonium sulfate and peroxide; N_{peroxide} and N_{aerosol} are the
 250 measured peroxide molar and calculated aerosol molar, respectively. More details about the
 251 iodometric-spectrophotometric procedures were described in previous work (Wang et al., 2018).
 252

253

254 **3 Results and discussion**

255 **3.1 SO₂ uptake and RH**

256 A positive relationship between γ_{SO_2} and RH (between 25 and 71 %) was observed for all types
257 of organic peroxides studied (Fig. 2). The positive dependence of the reactive uptake coefficient
258 of water-soluble gaseous species on RH has also been observed in other studies (Thornton et al.,
259 2003;Griffiths et al., 2009;Zhao et al., 2017;Zhang et al., 2019). Recently, the uptake behavior of
260 SO₂ onto soot, mineral dust and SOA were also shown to positively depend on RH (Zhang et al.,
261 2019;Zhao et al., 2017;Yao et al., 2019).

262 It is also noteworthy that an exponential dependence of SO₂ reactive uptake coefficient on RH
263 was observed in our study. γ_{SO_2} increases with increased relative humidity, which could even be
264 more significant under high RH regime. This is consistent with previous laboratory studies that
265 measured the reactive uptake coefficient of SO₂ onto aerosol to be exponentially dependent on
266 RH (Zhang et al., 2019;Yao et al., 2019). Additionally, multiple field campaigns have observed
267 significant correlation between particulate sulfate formation and ambient RH (Song et al.,
268 2019;Sun et al., 2013;Huang et al., 2020). Sun et al. (2013) observed faster sulfate formation rate
269 under humid conditions, proposing a significant impact of aerosol liquid water on sulfate
270 production during wintertime in Beijing. Zheng et al. (2015) reported a notably higher SOR
271 (molar ratio of sulfate to the sum of sulfate and SO₂) during wet period (RH>50 %), indicating
272 the importance of heterogeneous reactions to the secondary sulfur transformation with abundant
273 aerosol water content under humid conditions. In a recent study by Song et al. (2019), the rapid
274 sulfate formation rate observed under high RH conditions was found to be significantly higher
275 than atmospheric modeling results implemented with homogeneous SO₂ oxidation pathways,

276 which was later attributed to heterogeneous sulfate formation mechanisms. Multiple mechanisms
277 can potentially explain this observed γ_{SO_2} -RH dependence. An enhanced relative humidity would
278 result in a nonlinear increase of aerosol water content, which can lead to more SO_2 dissolved in
279 the aerosol aqueous phase (Seinfeld and Pandis, 2012). It should be noted that while the relative
280 humidity is varied systematically in these experiments, the relationship is more complex since
281 RH also affects other aerosol properties which can affect the uptake kinetics in turn. For
282 example, a higher aerosol liquid water content could dilute protons and thus lower the aerosol
283 acidity. In a study by Laskin et al. (2003), an enhanced uptake of SO_2 onto sea-salt particles was
284 observed with an increased aerosol alkalinity at high pH range.

285

286 **3.2 Dependence of SO_2 uptake on peroxide content and type**

287 As expected, the measured uptake rate of SO_2 is dependent on the particulate peroxide content in
288 the current study. Figure 3 shows that γ_{SO_2} is linearly proportional to the amount of particulate
289 peroxide for aerosol with similar volume-to-surface ratios and containing the same type of
290 organic peroxides. This positive relationship between γ_{SO_2} and condensed phase peroxide content
291 has also been inferred from experiments of SO_2 uptake onto α -pinene SOA (Yao et al., 2019),
292 where the peroxide content in α -pinene SOA was varied indirectly by introducing NO and
293 adjusting the branching ratio of the peroxide-yielding $\text{RO}_2+\text{HO}_2/\text{RO}_2$ pathway.

294 In addition to the amount of peroxide injected, the particulate fraction of organic peroxide
295 available for heterogeneous reaction is also influenced by gas-particle partitioning. As indicated
296 in Fig. 2, the reactive uptake coefficients of different organic peroxides vary amongst each other
297 by about an order of magnitude in the range of RH studied, despite the same amounts of peroxide
298 relative to ammonium sulfate initially in the atomizing solution. Based on our previous work

299 (Wang et al., 2019), the aqueous-phase rate constants for these organic peroxides with dissolved
300 S(IV) only vary by a factor of 2-3 and therefore cannot fully explain the observed difference in
301 uptake rates. Since vapour pressure vary considerably among the different peroxides in the
302 present study, gas-particle partitioning is likely to influence the amount of peroxide in the
303 particle phase that react with dissolved SO₂. The relative particulate peroxide content on filters
304 of the three peroxides collected from chamber experiments under RH 50 % without SO₂ uptake
305 were measured by the offline KI method (Fig. S7). Although the initial ratio of organic peroxide
306 to ammonium sulfate in the atomizing solution was nominally the same, we measured the highest
307 amount of particulate peroxide with 2-butanone peroxide (16.7 %), followed by cumene
308 hydroperoxide (12.7 %) and then tert-butyl hydroperoxide (3.8 %) using the offline iodometric
309 method. This trend in particulate peroxide content is consistent with the vapour pressures
310 calculated using the SIMPOL group contribution method (Pankow et al., 2008), with 2-butanone
311 peroxide being the least volatile, and tert-butyl hydroperoxide being the most volatile. Also, the
312 order of particle-phase peroxide content is consistent with the order of γ_{SO_2} observed, as shown in
313 Fig. 2. A simple visualization of these relationships between different peroxide characteristics
314 (number of peroxide groups, vapour pressure and aqueous-phase rate constants) and measured
315 γ_{SO_2} (at RH = 50 %) is illustrated in Fig. S7, which indicates higher γ_{SO_2} can be expected for
316 organic peroxides with multiple O-O groups, lower vapour pressures and higher aqueous phase
317 reactivities. It should be noted that the order of magnitude difference in experimentally measured
318 γ_{SO_2} among various organic peroxides (Fig.2) is still not fully explained when both volatility and
319 reaction kinetics are taken into account (Fig.S7), suggesting that the reactive uptake may be
320 influenced by other factors. In summary, for our current experiments where we nominally

321 maintained total injected amount of organic peroxide constant, measured γ_{SO_2} depends both on
322 reactivity and gas-particle partitioning of the organic peroxides.

323

324 **3.3 SO₂ uptake and aqueous phase kinetics**

325 Since the aqueous phase reaction rate constants between S(IV) and these model organic
326 peroxides have been measured previously (Wang et al., 2019), we can test our understanding of
327 the measured γ_{SO_2} using a simple model. By assuming the amount of SO₂ dissolved in the aerosol
328 is in equilibrium with the gas phase, the overall γ_{SO_2} can be expressed using the simplified
329 resistor model (Hanson et al., 1994):

330

$$331 \quad \frac{1}{\gamma} = \frac{1}{\alpha} + \frac{\bar{c}}{4HRT\sqrt{k^l D_l}} \frac{1}{\left[\coth(q) - \frac{1}{q}\right]} \quad (3)$$

332 where α is the mass accommodation coefficient, \bar{c} is the mean molecular speed of SO₂ (cm s⁻¹),
333 H is the effective Henry's law constant that includes both the dissolution of SO₂ and the
334 dissociation of H₂SO₃ (M atm⁻¹), R is the ideal gas constant (atm L mol⁻¹ K⁻¹), T is the
335 temperature (K), and the parameter q is used to describe the competition between the reaction
336 and diffusion of the dissolved gaseous species within a particle, which is further calculated as:

$$337 \quad q = r \sqrt{\frac{k^l}{D_l}} \quad (4)$$

338 where r is the radius (cm) of a given particle, D_l is the aqueous-phase diffusion coefficient (cm²
339 s⁻¹), k^l is the first order rate constant (s⁻¹) for the reaction. For experiments in the current study,
340 the calculated q values were consistently found to be far less than 1, which indicates a volume-
341 limited reaction regime. Combining with the assumption of a relatively fast mass
342 accommodation process compared with the bulk phase reaction, equation (3) can be further
343 simplified as to describes reactive uptake in the volume-limited regime:

344
$$\gamma = \frac{4HRT[\text{peroxide}]k^{\text{II}} V}{\bar{c} S} \quad (5)$$

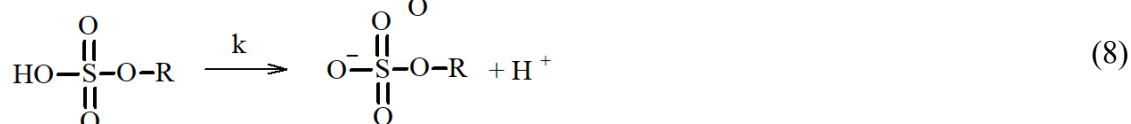
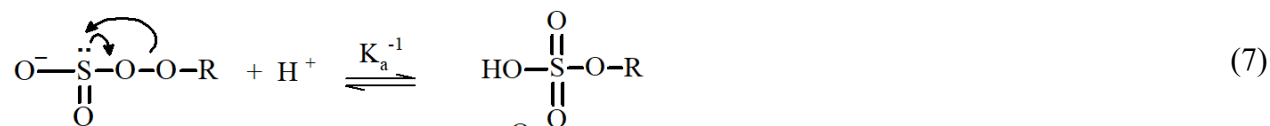
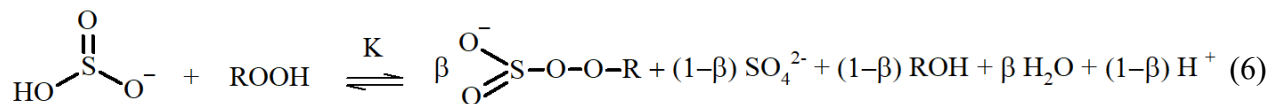
345 Here, we assume all the peroxides remain in the condensed phase upon atomizing and reaction
346 inside the chamber for the upper-bound prediction of γ_{SO_2} . [peroxide] represents the particle phase
347 concentration of total organic peroxide (M) based on the initial ratio between organic peroxide and
348 ammonium sulfate in the atomizing solution, and the aerosol water content output by E-AIM III
349 (Clegg et al., 1998), k^{II} is the second order reaction rate constant ($\text{M}^{-1} \text{s}^{-1}$), which we have
350 measured in the bulk phase at dilute concentrations previously (Wang et al., 2019), V/S is the ratio
351 between particle volume concentration ($\mu\text{m}^3 \text{cm}^{-3}$) and particle surface area concentration (μm^2
352 cm^{-3}) derived from SMPS measurements. As a result, the observed reactive uptake coefficient of
353 SO_2 can be compared to that predicted from the bulk phase reaction rate constant, and the results
354 are shown in Fig. 4 and Fig. S8. Overall, we noticed that this model captures the dependence of
355 γ_{SO_2} on peroxide content, but the modeled results were found to be generally 15-50 times lower
356 than the experimentally measured values (Fig. S8). The current γ_{SO_2} predictions are likely upper-
357 bound estimates since all the peroxides were assumed to stay in the condensed phase without
358 partitioning. As a result, this observed 15-50 times of discrepancy could even be larger if the
359 particulate peroxide content during the chamber experiments were lower due to partitioning.

360 It should be noted that the calculated γ_{SO_2} was based on reaction kinetics measured in dilute
361 solutions while the experimental γ_{SO_2} were measured directly from suspended particles. This large
362 difference in kinetics between those in aerosol and in dilute bulk solution suggests that this
363 multiphase interaction is strongly favored in the highly concentrated aerosol environment. One of
364 the potential explanations for this discrepancy could be liquid-liquid phase separation (LLPS) in
365 aerosol between organic peroxide and ammonium sulfate (Ciobanu et al., 2009; O'Brien et al.,
366 2015) such that SO_2 can directly interact with the acidic organic phase, where the concentration of

367 peroxides can be higher and the kinetics can be different from what we have measured in dilute
368 solution (Wang et al., 2019). However, LLPS is generally governed by the chemical composition
369 of the hydrophobic phase (Freedman, 2017). A higher level of oxygenation in organic aerosol is
370 related with higher hydrophilicity, which would favor a homogeneous particle instead of phase
371 separation. Previous studies showed that LLPS did not occur for organic coating with O:C above
372 0.8 (You et al., 2013; You et al., 2014). The LLPS phenomenon in simple organic–inorganic
373 mixtures can also be affected by the functional groups. The maximum O:C for LLPS could be 0.71
374 for organics with multiple carboxylic and hydroxyl groups but low aromatic content (Song et al.,
375 2012) while the 2-butanone peroxide we used for both γ_{SO_2} measurement and prediction in the
376 present study has multiple peroxide groups with an O:C value of 0.75. Particle size could also have
377 impacts on phase separation (Cheng et al., 2015). Particle diameters in the current study are mainly
378 under 200 nm while a previous study showed particles smaller than this size are less likely to
379 experience LLPS (Veghte et al., 2013). We therefore believe that LLPS is not likely to be
380 responsible for the enhanced uptake rate observed under these experimental conditions.

381 Another explanation is the high solute strength in the concentrated aerosol phase. Although the
382 aerosol water content for ammonium sulfate aerosol was found to be higher than that of malonic
383 acid aerosol under RH 50 %. As indicated in Fig. 4 and Fig. S8, the difference between the
384 measured and predicted γ_{SO_2} is larger for ammonium sulfate aerosol than for malonic acid.
385 Meanwhile, the calculated ionic strength in aerosol liquid phase under RH 50 % for ammonium
386 sulfate (40 mol kg^{-1}) is significantly larger than that of malonic acid (0.45 mol kg^{-1}). It has been
387 previously reported that the reaction rate between sulfite and hydrogen peroxide in aqueous phase
388 increases with ionic strength (Maaß et al., 1999). Based on the reaction mechanisms proposed for

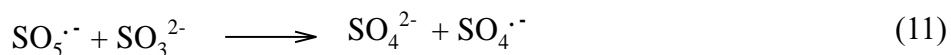
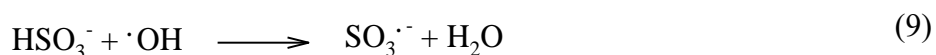
389 dissolved SO₂ and hydrogen peroxide (Halperin and Taube, 1952), we speculate the reaction
 390 between aqueous phase S(IV) and organic peroxides to follow a similar mechanism:



391
 392 where the overall rate constant is equal to $k \frac{K}{K_a}$, assuming fast equilibrium steps for reactions 6 and
 393 7. Dissociated solutes are surrounded by an extended solvation shell which could affect the
 394 reaction rates (Herrmann, 2003). Fewer available free water molecules would therefore shift the
 395 equilibrium to the right in equation (6). Additionally, higher ionic strength also corresponds to an
 396 increased concentration of electrolytes in the aqueous phase, which could hinder the dissociation
 397 of the peroxy monosulfurous acid and shift the equilibrium in equation (7) to the right. In recent
 398 work by Liu et al. (2020), the rate of S(IV) oxidation by H₂O₂ can be enhanced by up to a factor
 399 of 50 in aerosol aqueous phase compared to that of dilute solution. The highest ionic strength at
 400 which such enhancement was measured for the H₂O₂ oxidation pathway was 15 mol kg⁻¹ (Liu et
 401 al., 2020).

402 Whereas the above analysis is based on the assumption that all the chemistry occurs in the bulk
 403 component of the particle, it is also possible that some component of the reaction occurs at the gas-
 404 particle interface and the overall kinetics can be affected by interfacial characteristics. For example,
 405 an enhanced ionic strength in the aerosol phase can also impact the interfacial reaction mechanisms.
 406 Previous study has shown evidence that interfacial chemistry is important for SO₂ oxidation in the

407 aerosol phase (Laskin et al., 2003). With higher ionic strength, anions partitioning to the air-liquid
 408 interface can promote the overall reaction kinetics via proton transfer and thus accelerate the
 409 interfacial chemistry (Knipping et al., 2000; Mishra et al., 2012; Mekic et al., 2018; Mekic et al.,
 410 2020; Wei et al., 2018; Ruiz-Lopez et al., 2020). In addition to the catalytic effects of protons
 411 indicated in Eqn.6-8, Hung et al. (2015, 2018) observed significant $\text{SO}_3^{\cdot-}$ signal at the acidic
 412 microdroplet surface, which can promote sulfate formation via radical propagation chain initiated
 413 by surrounding radicals and molecular oxygen (Eqn. 9-12):



414
 415 where the hydroxy radical can potentially be produced from decomposition of the labile organic
 416 peroxide in our system (Tong et al., 2016). However, we cannot distinguish whether the interfacial
 417 protons promote sulfate formation by catalyze the peroxide S(IV) oxidation pathway or the sulfur
 418 radical pathway at the current stage. In the recent study by Wei et al. (2018), a pH gradient was
 419 observed for phosphate-buffered aerosol droplets with the proton accumulated at the interface.
 420 Base on the pH-dependent aqueous phase kinetics measured in our previous work (Wang et al.,
 421 2019), such interfacial proton accumulation could potentially explain the enhanced kinetics we
 422 observed for aerosol in the current study. However, the chemical compositions are quite different.
 423 While phosphate-buffered particles were studied in Wei et al. (2018), acidic ammonium sulfate
 424 aerosol was used in our study. Also, the particle size in Wei et al. (2018) is significantly larger (20
 425 μm) than what was studied in the current study (200 nm). Thus, it should be noted that there is no

426 direct evidence from the current study showing the relationship between the interfacial properties
427 and γ_{SO_2} , and future studies are warranted.

428 Therefore, while more studies are needed to clearly delineate the roles of ionic strength, interfacial
429 activity, bulk reactivity, and particle phase state quantitatively, the enhancement of SO_2 oxidation
430 kinetics by highly concentrated aerosol particles compared to dilute aqueous solutions are
431 concluded to be large (factor of 15-50) for the experimental conditions in the current study.

432

433 **3.4 SO_2 uptake and aerosol pH**

434 As indicated by the proposed reaction mechanisms (Eqn. 6-8), protons are important reaction
435 intermediates for this SO_2 oxidation pathway. Previously, the aqueous phase reaction rate
436 constants between organic peroxides and dissolved SO_2 were measured to be pH dependent
437 (Wang et al., 2019). Moreover, the dissolution equilibrium of SO_2 into aqueous phase is also pH
438 sensitive (Seinfeld and Pandis, 2012). Besides, many studies have shown that the uptake kinetics
439 for gaseous species can be affected by the condensed phase pH (Shi et al., 1999; Gaston et al.,
440 2014; Drozd et al., 2013; Jang and Kamens, 2001; Liu et al., 2015). Reactive uptake of ammonia
441 was observed to depend on condensed phase acidity (Shi et al., 1999). Heterogeneous
442 condensation of isoprene-derived epoxydiol onto seed aerosol was found to increase with proton
443 concentration (Gaston et al., 2014). In the current study, the potential impact from particle phase
444 pH on γ_{SO_2} was explored by adding HCl into the atomizing solution. To estimate the particle
445 phase pH, two different methods associated with two different assumptions were used. In the
446 first scenario, the aerosol pH in each experiment was estimated using the E-AIM III model
447 (Clegg et al., 1998) based on the initial molar ratios of inorganic species (H^+ , NH_4^+ , SO_4^{2-} , Cl^-) in
448 the atomizing solution and measured RH (around 50 %). In the second scenario, the additional

449 sulfate formed from reactive uptake of SO₂ was taken into consideration. The partitioning of HCl
450 was allowed in the model simulation for both scenarios. The formation of sulfate would enhance
451 the proton concentration in the aerosol liquid phase thus lower the aerosol pH. The average pH
452 during the SO₂ uptake process is likely in between these two extremes.

453 Figure 5 shows the measured reactive uptake coefficients of SO₂ as a function of the calculated
454 pH. The reactive uptake coefficient was found to weakly increase with decreasing pH, which is
455 consistent with acid-catalyzed reactions between peroxides and dissolved SO₂ as measured in the
456 bulk phase (Lind et al., 1987; Wang et al., 2019). γ_{SO_2} was also predicted for the same range of
457 pH based on Eqn. 5 and the pH-dependent bulk-phase reaction rate constants measured
458 previously (Wang et al., 2019). Indicated by Fig. 5, the measured γ_{SO_2} again exceeds the
459 predicted γ_{SO_2} by about a factor of 50, which is consistent with what we reported earlier and is
460 likely due to the effects of aerosol ionic strength.

461 Unlike the observed γ_{SO_2} , however, the predicted γ_{SO_2} does not exhibit a monotonic trend. γ_{SO_2} is
462 expected to decrease with decreasing pH at high pH (>2) as the effective Henry's law constant of
463 SO₂ decreases with higher acidity (Seinfeld and Pandis, 2012). γ_{SO_2} is not expected to increase
464 with decreasing pH until pH is below 2 where the acidity enhancement in reaction rate constant
465 exceeds the decrease in SO₂ solubility. As illustrated earlier, extrapolating dilute aqueous-phase
466 kinetics to the highly concentrated aerosol requires considering effects from high solute strength.
467 Solute strength may change the pH dependence of γ_{SO_2} in two ways. First, the solubility of SO₂
468 may decrease and become less dependent on pH as ionic strength increases (Rodríguez-Sevilla et
469 al., 2002). A former study (Leng et al., 2015) has shown that the effective Henry's law of
470 triethylamine decreases with increased ionic strength. Another potential explanation is that the
471 aqueous phase reaction rate constant can be more pH-dependent at high ionic strengths than what

472 we measured previously in dilute solutions. In either case, the inflection of the predicted γ_{SO_2}
473 would change and γ_{SO_2} could become more negatively dependent on pH ($d[\gamma_{\text{SO}_2}]/d[\text{pH}]$ becomes
474 less positive in the high pH range and/or more negative in the low pH range), which would
475 match more closely with the observed dependence. It should also be noted that there are
476 substantial uncertainties in estimating pH values, originating from the partitioning of organics,
477 organic-inorganic phase separations, mixing state of specific ions, uncertain activity coefficients
478 and the propagation of RH uncertainties (Clegg et al., 2008; Fountoukis et al., 2009; Guo et al.,
479 2016). Also, the reactive uptake is a dynamic process and will influence aerosol pH in turn upon
480 sulfate formation. In summary, while the magnitude of predicted γ_{SO_2} is consistent with our
481 expected values (after accounting for the enhancement by high aerosol solute strength), we
482 cannot fully explain the dependence of γ_{SO_2} on aerosol pH at the current stage. Future studies
483 should investigate how the effective Henry's law of SO_2 and pH dependence of reaction rate
484 constants vary in aerosol liquid phase with high solute strength in order to have a more
485 comprehensive understanding of the relationship between γ_{SO_2} and aerosol pH.

486

487 **3.4 SO₂ uptake onto SOA**

488 γ_{SO_2} was measured for a few model SOA systems, as organic peroxides are abundant in SOA
489 (Surratt et al., 2006; Kautzman et al., 2009; Krapf et al., 2016; Bonn et al., 2004). Here we studied
490 SOA formed from monoterpene ozonolysis and toluene photooxidation. It should be noted that
491 for the γ_{SO_2} measurements of toluene SOA, a strong hydrocarbon interference was observed with
492 the SO_2 analyzer, likely stemming from the high concentrations of gas-phase aromatic
493 compounds. A rough estimate of the uptake rate for toluene SOA from aerosol mass
494 spectrometer sulfate measurements is provided in the SI (Section 1). The reactive uptake

495 coefficient of SO₂ onto Saharan mineral dust was reported on the order of 10⁻⁵ (Adams et al.,
496 2005). γ_{SO_2} onto dust with the coexistence of NO₂ and NH₃ under various RH conditions were
497 measured to be 10⁻⁷ to 10⁻⁵ (Zhang et al., 2019). For a variety of metal oxides, SO₂ reactive
498 uptake coefficients were quantified to be between 10⁻⁶ and 10⁻⁴ (Usher et al., 2002; Fu et al.,
499 2007; Shang et al., 2010). More recently, γ_{SO_2} studied for heterogeneous sulfate formation by
500 photolysis of particulate nitrate were reported in the range of 10⁻⁶ to 10⁻⁵ (Gen et al., 2019). As
501 shown in Fig. 6, γ_{SO_2} for all SOA systems were measured to be on the order of 10⁻⁴. Similar γ_{SO_2}
502 values on the order of 10⁻⁴ were measured for α -pinene SOA by Yao et al. (2019), and 10⁻⁵ for
503 limonene SOA estimated from the chamber study by Ye et al. (2018). The reaction products
504 from this SOA and SO₂ interaction will be reported in a separate study.

505

506 **4. Atmospheric Implications**

507 Oxidation of atmospheric hydrocarbons produces reactive intermediates that can potentially
508 interact with SO₂ and form particulate sulfate, contributing to PM formation and growth (Berndt
509 et al., 2015; Mauldin et al., 2012; Yao et al., 2019). Organic peroxides generated from both
510 biogenic and anthropogenic hydrocarbon emissions are abundant in submicron aerosol. Given
511 that they are highly reactive with relatively short lifetimes (Bonn et al., 2004; Krapf et al.,
512 2016; Qiu et al., 2020), these species could serve as important condensed phase oxidants for gas
513 phase SO₂. Combining laboratory measurements and model predictions, the current study
514 investigated heterogeneous reactions between SO₂ and particulate organic peroxide. The
515 measured γ_{SO_2} for organic peroxide containing aerosol ranges from 10⁻⁵ to 10⁻² in this study.
516 Based on the modeling work by Wang et al. (2014), adding an SO₂ uptake pathway to GEOS-
517 Chem with a reactive uptake coefficient of 10⁻⁴ could improve the surface sulfate prediction by

518 more than 50 % during a severe haze episode over North China (RH 50 %), suggesting the
519 potential importance of this multiphase reaction pathway, especially when SOA is the dominant
520 component in particulate matter.

521 The dependence of the heterogeneous kinetics on RH, aerosol pH, peroxide type, and peroxide
522 content were also evaluated. The experimentally measured γ_{SO_2} was found to be consistently
523 higher than that predicted from reaction kinetics with organic peroxides in the dilute aqueous
524 phase. This discrepancy can be potentially explained by the effects of high ionic strength
525 presented in the aerosol, suggesting that the impact from highly concentrated solutes needs to be
526 taken into consideration when applying aqueous phase kinetics to aerosol multiphase chemistry,
527 especially for particles containing strong electrolytes. We also observed that the kinetics of this
528 multiphase reaction exhibit a weak dependence on pH. Increasing the condensed-phase acidity
529 may enhance the heterogeneous rate constant at low pH, and while this pH dependence is
530 consistent with that of the aqueous phase reaction rate constant measured previously, it is not
531 consistent with the decrease of effective Henry's law constant of SO_2 along with enhanced
532 acidity. Also, it is likely that within the uncertainties, there may not be an observable γ_{SO_2} -pH
533 trend. Currently, we are not able to fully explain the pH dependence, and further studies are
534 warranted. Particle phase peroxide content was observed to be linearly correlated with γ_{SO_2} .
535 Moreover, γ_{SO_2} measured for 2-butanone peroxide was found to be orders of magnitude higher
536 than that of cumene hydroperoxide and tert-butyl hydroperoxide. The difference in γ_{SO_2} among
537 various types of organic peroxides can be partially explained by their condensed-phase reactivity
538 and gas-particle partitioning.

539 In general, we found the observed γ_{SO_2} in this study can be summarized using the following
540 semiempirical multilinear relationship:

541
$$\log \gamma = -1.7 + 0.0024 \times k'' + 0.46 \times PAS + 0.024 \times RH - 1.9 \times Vp \quad (13)$$

542 where γ is the reactive uptake coefficient, k'' is the aqueous phase S(IV) oxidation rate constant
543 ($M^{-1} s^{-1}$), PAS is the molar ratio between particulate peroxide and ammonium sulfate in the
544 atomizing solution, which is a proxy for the amount of peroxide in both gas and particle phases
545 applied in the current study, RH is the relative humidity (%), Vp is the vapour pressure (kPa) of
546 the peroxide. Figure 7 illustrates the degree to which this semi-empirical expression describes the
547 experimental data for ammonium sulfate aerosol mixed with the three types of organic peroxides.
548 Residual evaluations of this multilinear regression can be found Fig. S9. We caution that this
549 equation is not directly applicable to atmospheric models in its current form, especially since the
550 particle phase peroxide content (PAS) value we applied as input is a calculated value, rather than
551 a measurement. However, it illustrates the internal consistency of our experimental results across
552 a range of RH, peroxide content, and aqueous phase reactivities, which are the key variables for
553 uptake rates. Better understanding of ionic strengths and pH in aerosol, either through modeling
554 or direct measurements of these variables, is needed to establish the coefficient dependence.
555 Future studies should be focused on exploring γ_{SO_2} and the reaction products for various types of
556 SOA as well as ambient particles under atmospherically relevant conditions, evaluating the
557 underlying impacts from photochemical condition, chemical composition, particle morphology,
558 ionic strength and interfacial properties on this multiphase physicochemical process. Overall,
559 γ_{SO_2} presented in our study and its relationship with ambient RH, aerosol pH, ionic strength,
560 particulate peroxide content and type could provide a framework for the implementation of this
561 heterogeneous mechanism in atmospheric models to have a better understanding of ambient
562 sulfate formation and particle growth.

563

564 *Author contributions*

565 A.W.H. C. and S.W. designed the study. S.W., T. L., and J. J. performed the experiments. S.W.,
566 A.W.H. C., T. L., and J. J. analyzed data. S.W. and A.W.H. C. wrote the manuscript with the
567 input from all co-authors.

568

569 *Data availability*

570 All data presented in this study are available in the supplemental material and have been
571 deposited in figshare.

572

573 *Associated content*

574 Supporting Information.

575

576 *Competing interests*

577 The authors declare no competing financial interest.

578

579 *Acknowledgements*

580 This work was supported by Natural Sciences and Engineering Research Council Discovery Grant.

581 The authors would like to thank Dr. Greg Evans, Dr. Yue Zhao and Dr. Christopher Lim for helpful
582 comments and discussions. Special thanks to SOCAAR for providing the SO₂ analyzer.

583

584

585

586

587

588 **Reference**

- 589 Abbatt, J. P. D., Lee, A. K. Y., and Thornton, J. A.: Quantifying trace gas uptake to tropospheric
590 aerosol: recent advances and remaining challenges, *Chem. Soc. Rev.*, 41, 6555–6581,
591 <https://doi.org/10.1039/c2cs35052a>, 2012.
- 592 Adams, J. W., Rodriguez, D., and Cox, R. A.: The uptake of SO₂ on Saharan dust: a flow tube
593 study, *Atmos. Chem. Phys.*, 5, 2643–2676, doi:10.5194/acp-5-2643-2005, 2005.
- 594 Andreae, M.O., Afchine, A., Albrecht, R., Holanda, B.A., Artaxo, P., Barbosa, H.M., Borrmann,
595 S., Cecchini, M.A., Costa, A., Dollner, M. and Fütterer, D.: Aerosol characteristics and particle
596 production in the upper troposphere over the Amazon Basin, *Atmos. Chem. Phys.*, 18, 921–961,
597 2018.
- 598 Atkinson, R., and Arey, J.: Atmospheric degradation of volatile organic compounds, *Chem.*
599 *Rev.*, 103, 4605-4638, 2003.
- 600 Berndt, T., Richters, S., Kaethner, R., Voigtländer, J., Stratmann, F., Sipilä, M., Kulmala, M.,
601 and Herrmann, H.: Gas-phase ozonolysis of cycloalkenes: Formation of highly oxidized RO₂
602 radicals and their reactions with NO, NO₂, SO₂, and other RO₂ radicals, *J. Phys. Chem. A*, 119,
603 10336-10348, 10.1021/acs.jpca.5b07295, 2015.
- 604 Bianchi, F., Kurtén, T., Riva, M., Mohr, C., Rissanen, M. P., Roldin, P., Berndt, T., Crouse, J.
605 D., Wennberg, P. O., Mentel, T. F., Wildt, J., Junninen, H., Jokinen, T., Kulmala, M., Worsnop,
606 D. R., Thornton, J. A., Donahue, N., Kjaergaard, H. G., and Ehn, M.: Highly oxygenated organic
607 molecules (HOM) from gas-phase autoxidation involving peroxy radicals: A key contributor to
608 atmospheric aerosol, *Chem. Rev.*, 119, 3472-3509, 10.1021/acs.chemrev.8b00395, 2019.
- 609 Bonn, B., von Kuhlmann, R., and Lawrence, M. G.: High contribution of biogenic
610 hydroperoxides to secondary organic aerosol formation, *Geophys. Res. Lett.*, 31, L10108,
611 <https://doi.org/10.1029/2003GL019172>, 2004.
- 612 Chen, Q., Farmer, D. K., Schneider, J., Zorn, S. R., Heald, C. L., Karl, T. G., Guenther, A.,
613 Allan, J. D., Robinson, N., Coe, H., Kimmel, J. R., Pauliquevis, T., Borrmann, S., Pöschl, U.,
614 Andreae, M. O., Artaxo, P., Jimenez, J. L., and Martin, S. T.: Mass spectral characterization of
615 submicron biogenic organic particles in the Amazon Basin, *Geophys. Res. Lett.*, 36, L20806,
616 <https://doi.org/10.1029/2009GL039880>, 2009.
- 617 Chen, T., Chu, B., Ge, Y., Zhang, S., Ma, Q., He, H., and Li, S.-M.: Enhancement of aqueous
618 sulfate formation by the coexistence of NO₂/NH₃ under high ionic strengths in aerosol water,
619 *Environ. Pollut.*, 252, 236-244, <https://doi.org/10.1016/j.envpol.2019.05.119>, 2019.
- 620 Cheng, Y., Su, H., Koop, T., Mikhailov, E., and Pöschl, U.: Size dependence of phase transitions
621 in aerosol nanoparticles, *Nat. Commun.*, 6, 5923, 10.1038/ncomms6923, 2015.
- 622 Cheng, Y. F., Zheng, G. J., Wei, C., Mu, Q., Zheng, B., Wang, Z. B., Gao, M., Zhang, Q., He, K.
623 B., Carmichael, G., Pöschl, U., and Su, H.: Reactive nitrogen chemistry in aerosol water as a
624 source of sulfate during haze events in China, *Sci. Adv.*, 2, e1601530, 2016.
- 625 Ciobanu, V. G., Marcolli, C., Krieger, U. K., Weers, U., and Peter, T.: Liquid-liquid phase
626 separation in mixed organic/inorganic aerosol particles, *J. Phys. Chem. A*, 113, 10966–10978,
627 2009.

628 Clegg, S. L., Brimblecombe, P., and Wexler, A. S.: Thermodynamic model of the system
629 $\text{H}^+ - \text{NH}_4^+ - \text{Na}^+ - \text{SO}_4^{2-} - \text{NO}_3^- - \text{Cl}^- - \text{H}_2\text{O}$ at 298.15 K, *J. Phys. Chem. A*, 102, 2155–2171,
630 <https://doi.org/10.1021/jp973043j>, 1998.

631 Clegg, S. L., Kleeman, M. J., Griffin, R. J., and Seinfeld, J. H.: Effects of uncertainties in the
632 thermodynamic properties of aerosol components in an air quality model – Part 1: Treatment of
633 inorganic electrolytes and organic compounds in the condensed phase, *Atmos. Chem. Phys.*, 8,
634 1057–1085, <http://www.atmos-chem-phys.net/8/1057/2008/>, 2008.

635 Ding, J., Zhao, P., Su, J., Dong, Q., Du, X., and Zhang, Y.: Aerosol pH and its driving factors in
636 Beijing, *Atmos. Chem. Phys.*, 19, 7939–7954, 10.5194/acp-19-7939-2019, 2019.

637 Docherty, K. S., Wu, W., Lim, Y. B., and Ziemann, P. J.: Contributions of organic peroxides to
638 secondary aerosol formed from reactions of monoterpenes with O_3 , *Environ. Sci. Technol.*, 39,
639 4049–4059, 2005.

640 Dovrou, E., Rivera-Rios, J. C., Bates, K. H., and Keutsch, F. N.: Sulfate formation via cloud
641 processing from isoprene hydroxyl hydroperoxides (ISOPOOH), *Environ. Sci. Technol.*, 53,
642 12476–12484, 10.1021/acs.est.9b04645, 2019.

643 Drozd, G. T., Woo, J. L., and McNeill, V. F.: Self-limited uptake of α -pinene oxide to acidic
644 aerosol: the effects of liquid-liquid phase separation and implications for the formation of
645 secondary organic aerosol and organosulfates from epoxides, *Atmos. Chem. Phys.*, 13, 8255–
646 8263, doi:10.5194/acp-13-8255-2013, 2013.

647 Epstein, S. A., Blair, S. L., and Nizkorodov, S. A.: Direct photolysis of α -pinene ozonolysis
648 secondary organic aerosol: effect on particle mass and peroxide content, *Environ. Sci. Technol.*,
649 48, 11251–11258, 2014.

650 Fairlie, T. D., Jacob, D. J., Dibb, J. E., Alexander, B., Avery, M. A., van Donkelaar, A., and
651 Zhang, L.: Impact of mineral dust on nitrate, sulfate, and ozone in transpacific Asian pollution
652 plumes, *Atmos. Chem. Phys.*, 10, 3999–4012, doi:10.5194/acp-10-3999-2010, 2010.

653 Fountoukis, C., Nenes, A., Sullivan, A., Weber, R., Van Reken, T., Fischer, M., Matas, E.,
654 Moya, M., Farmer, D., and Cohen, R. C.: Thermodynamic characterization of Mexico City
655 aerosol during MILAGRO 2006, *Atmos. Chem. Phys.*, 9, 2141–2156, 2009.

656 Freedman, M. A.: Phase separation in organic aerosol, *Chem. Soc. Rev.*, 46, 7694–7705,
657 <https://doi.org/10.1039/C6CS00783J>, 2017.

658 Fu, H. B., Wang, X., Wu, H. B., Yin, Y., and Chen, J. M.: Heterogeneous uptake and oxidation
659 of SO_2 on iron oxides, *J. Phys. Chem. C*, 111, 6077–6085, 2007.

660 Gao, M., Carmichael, G. R., Wang, Y., Saide, P. E., Yu, M., Xin, J., Liu, Z., and Wang, Z.:
661 Modeling study of the 2010 regional haze event in the North China Plain, *Atmos. Chem. Phys.*,
662 16, 1673–1691, <https://doi.org/10.5194/acp-16-1673-2016>, 2016.

663 Gaston, C. J., Riedel, T. P., Zhang, Z., Gold, A., Surratt, J. D., and Thornton, J. A.: Reactive
664 uptake of an isoprene-derived epoxydiol to submicron aerosol particles, *Environ. Sci. Technol.*,
665 48, 11178–11186, 10.1021/es5034266, 2014.

666 Gen, M., Zhang, R., Huang, D. D., Li, Y., and Chan, C. K.: Heterogeneous SO_2 oxidation in
667 sulfate formation by photolysis of particulate nitrate, *Environ. Sci. Tech. Lett.*, 6, 86–91,
668 <https://doi.org/10.1021/acs.estlett.8b00681>, 2019.

669 Griffiths, P. T., Badger, C. L., Cox, R. A., Folkers, M., Henk, H. H., and Mentel, T. F.: Reactive
670 uptake of N_2O_5 by aerosols containing dicarboxylic acids. Effect of particle phase, composition,
671 and nitrate content, *J. Phys. Chem. A*, 113, 5082-5090, [10.1021/jp8096814](https://doi.org/10.1021/jp8096814), 2009.

672 Gunz, D. W. and Hoffmann, M. R.: Atmospheric chemistry of peroxides: A review, *Atmos.*
673 *Environ.*, 24A, 1601–1633, [https://doi.org/10.1016/0960-1686\(90\)90496-A](https://doi.org/10.1016/0960-1686(90)90496-A), 1990.

674 Guo, H., Sullivan, A. P., Campuzano-Jost, P., Schroder, J. C., LopezHilfiker, F. D., Dibb, J. E.,
675 Jimenez, J. L., Thornton, J. A., Brown, S. S., Nenes, A., and Weber, R. J.: Fine particle pH and
676 the partitioning of nitric acid during winter in the northeastern United States, *J. Geophys. Res.*
677 *Atmos.*, 121, 10355–10376, <https://doi.org/10.1002/2016JD025311>, 2016.

678 Guo, H., Weber, R. J., and Nenes, A.: High levels of ammonia do not raise fine particle pH
679 sufficiently to yield nitrogen oxide-dominated sulfate production, *Sci. Rep.*, 7, 12109, 2017.

680 Hallquist, M., Wenger, J. C., Baltensperger, U., Rudich, Y., Simpson, D., Claeys, M., Dommen,
681 J., Donahue, N. M., George, C., Goldstein, A. H., Hamilton, J. F., Herrmann, H., Hoffmann, T.,
682 Iinuma, Y., Jang, M., Jenkin, M. E., Jimenez, J. L., Kiendler-Scharr, A., Maenhaut, W.,
683 McFiggans, G., Mentel, Th. F., Monod, A., Prévôt, A. S. H., Seinfeld, J. H., Surratt, J. D.,
684 Szmigielski, R., and Wildt, J.: The formation, properties and impact of secondary organic
685 aerosol: current and emerging issues, *Atmos. Chem. Phys.*, 9, 5155–5236, 2009.

686 Halperin, J., and Taube, H.: The transfer of oxygen atoms in oxidation—reduction reactions. IV.
687 The reaction of hydrogen peroxide with sulfite and thiosulfate, and of oxygen, manganese
688 dioxide and of permanganate with sulfite, *J. Am. Chem. Soc.*, 74, 380-382, 1952.

689 Hanson, D. R., Ravishankara, A. R., and Solomon, S.: Heterogeneous reactions in sulfuric acid
690 aerosols: A framework for model calculations, *J. Geophys. Res.*, 99, 3615, [https://doi.org/](https://doi.org/10.1029/93JD02932)
691 [10.1029/93JD02932](https://doi.org/10.1029/93JD02932), 1994.

692 Hartz, K. E. H., Rosenorn, T., Ferchak, S. R., Raymond, T. M., Bilde, M., Donahue, N. M., and
693 Pandis, S. N.: Cloud condensation nuclei activation of monoterpene and sesquiterpene
694 secondary organic aerosol, *J. Geophys. Res.-Atmos.*, 110(D14), D14208, 2005.

695 He, L.-Y., Huang, X.-F., Xue, L., Hu, M., Lin, Y., Zheng, J., Zhang, R., and Zhang, Y.-H.:
696 Submicron aerosol analysis and organic source apportionment in an urban atmosphere
697 in Pearl River Delta of China using high-resolution aerosol mass spectrometry, *J. Geophys. Res.*
698 *Atmos.*, 116, D12304, <https://doi.org/10.1029/2010JD014566>, 2011.

699 Herrmann, H.: Kinetics of aqueous phase reactions relevant for atmospheric chemistry, *Chem.*
700 *Rev.*, 103, 4691–4716, 2003.

701 Hildebrandt, L., Donahue, N. M., Pandis, S. N.: High formation of secondary organic aerosol
702 from the photo-oxidation of toluene, *Atmos. Chem. Phys.*, 9, 2973–2986, 2009.

703 Huang, L., An, J., Koo, B., Yarwood, G., Yan, R., Wang, Y., Huang, C., and Li, L.: Sulfate
704 formation during heavy winter haze events and the potential contribution from heterogeneous
705 $\text{SO}_2 + \text{NO}_2$ reactions in the Yangtze River Delta region, China, *Atmos. Chem. Phys.*, 19, 14311-
706 14328, [10.5194/acp-19-14311-2019](https://doi.org/10.5194/acp-19-14311-2019), 2019.

707 Huang, L., Coddens, E. M., and Grassian, V. H.: Formation of organosulfur compounds from
708 aqueous phase reactions of S (IV) with methacrolein and methyl vinyl ketone in the presence of
709 transition metal ions, *ACS Earth Space Chem.*, 3, 1749-1755, 2019.

710 Huang, L., Liu, T. and Grassian, V. H.: Radical-initiated formation of aromatic organosulfates
711 and sulfonates in the aqueous phase. *Environ. Sci. Technol.*, 54, 11857–11864, 2020.

712 Huang, R. J., Zhang, Y. L., Bozzetti, C., Ho, K. F., Cao, J. J., Han, Y. M., Daellenbach, K. R.,
713 Slowik, J. G., Platt, S. M., Canonaco, F., Zotter, P., Wolf, R., Pieber, S. M., Bruns, E. A., Crippa,
714 M., Ciarelli, G., Piazzalunga, A., Schwikowski, M., Abbaszade, G., Schnelle-Kreis, J.,
715 Zimmermann, R., An, Z., Szidat, S., Baltensperger, U., Haddad, I. E., and Prevot, A. S. H.: High
716 secondary aerosol contribution to particulate pollution during haze events in China, *Nature*, 514,
717 218–222, 2014.

718 Huang, R. J., He, Y., Duan, J., Li, Y., Chen, Q., Zheng, Y., Chen, Y., Hu, W., Lin, C., Ni, H.,
719 Dai, W., Cao, J., Wu, Y., Zhang, R., Xu, W., Ovadnevaite, J., Ceburnis, D., Hoffmann, T., and
720 O'Dowd, C. D.: Contrasting sources and processes of particulate species in haze days with low
721 and high relative humidity in wintertime Beijing, *Atmos. Chem. Phys.*, 20, 9101-9114,
722 10.5194/acp-20-9101-2020, 2020.

723 Hung, H. M. and Hoffmann, M. R.: Oxidation of gas-phase SO₂ on the surfaces of acidic
724 microdroplets: Implications for sulfate and sulfate radical anion formation in the atmospheric
725 liquid phase, *Environ. Sci. Technol.*, 49, 13768–13776, 2015.

726 Hung, H. M., Hsu, M. N., and Hoffmann, M. R.: Quantification of SO₂ oxidation on interfacial
727 surfaces of acidic micro-droplets: Implication for ambient sulfate formation, *Environ. Sci.*
728 *Technol.*, 52, 9079–9086, <https://doi.org/10.1021/acs.est.8b01391>, 2018.

729 Jang, M., and Kamens, R. M.: Atmospheric secondary aerosol formation by heterogeneous
730 reactions of aldehydes in the presence of a sulfuric acid aerosol catalyst, *Environ. Sci. Technol.*,
731 35, 4758-4766, 10.1021/es010790s, 2001.

732 Jimenez, J. L., Canagaratna, M. R., Donahue, N. M., Prevot, A. S. H., Zhang, Q., Kroll, J. H.,
733 DeCarlo, P. F., Allan, J. D., Coe, H., Ng, N. L., Aiken, A. C., Docherty, K. S., Ulbrich, I. M.,
734 Grieshop, A. P., Robinson, A. L., Duplissy, J., Smith, J. D., Wilson, K. R., Lanz, V. A., Hueglin,
735 C., Sun, Y. L., Tian, J., Laaksonen, A., Raatikainen, T., Rautiainen, J., Vaattovaara, P., Ehn, M.,
736 Kulmala, M., Tomlinson, J. M., Collins, D. R., Cubison, M. J., Dunlea, J., Huffman, J. A.,
737 Onasch, T. B., Alfarra, M. R., Williams, P. I., Bower, K., Kondo, Y., Schneider, J., Drewnick,
738 F., Borrmann, S., Weimer, S., Demerjian, K., Salcedo, D., Cottrell, L., Griffin, R., Takami, A.,
739 Miyoshi, T., Hatakeyama, S., Shimono, A., Sun, J. Y., Zhang, Y. M., Dzepina, K., Kimmel,
740 J. R., Sueper, D., Jayne, J. T., Herndon, S. C., Trimborn, A. M., Williams, L. R., Wood, E. C.,
741 Middlebrook, A. M., Kolb, C. E., Baltensperger, U., and Worsnop, D. R.: Evolution of organic
742 aerosols in the atmosphere, *Science*, 326, 1525–1529, <https://doi.org/10.1126/science.1180353>,
743 2009.

744 Kautzman, K., Surratt, J., Chan, M., Chan, A., Hersey, S., Chhabra, P., Dalleska, N., Wennberg,
745 P., Flagan, R., and Seinfeld, J.: Chemical composition of gas-and aerosol-phase products from
746 the photooxidation of naphthalene, *J. Phys. Chem. A*, 114, 913-934, 2009.

747 Knipping, E. M., Lakin, M. J., Foster, K. L., Jungwirth, P., Tobias, D. J., Gerber, R. B., Dabdub,
748 D., and Finlayson-Pitts, B. J.: Experiments and simulations of ion-enhanced interfacial chemistry
749 on aqueous NaCl aerosols, *Science*, 288, 301, 10.1126/science.288.5464.301, 2000.

750 Krapf, M., El Haddad, I., Bruns, E. A., Molteni, U., Daellenbach, K. R., Prévôt, A. S.,
751 Baltensperger, U., and Dommen, J.: Labile peroxides in secondary organic aerosol, *Chem*, 1,
752 603-616, 2016.

753 Laskin, A., Gaspar, D. J., Wang, W., Hunt, S. W., Cowin, J. P., Colson, S. D., and Finlayson-
754 Pitts, B. J.: Reactions at interfaces as a source of sulfate formation in sea-salt particles, *Science*,
755 301, 340, 10.1126/science.1085374, 2003.

756 Leng, C. B., Roberts, J. E., Zeng, G., Zhang, Y. H., and Liu, Y.: Effects of temperature, pH, and
757 ionic strength on the Henry's law constant of triethylamine, *Geophys. Res. Lett.*, 42, 3569-3575,
758 10.1002/2015gl063840, 2015.

759 Li, G., Bei, N., Cao, J., Huang, R., Wu, J., Feng, T., Wang, Y., Liu, S., Zhang, Q., Tie, X., and
760 Molina, L. T.: A possible pathway for rapid growth of sulfate during haze days in China, *Atmos.*
761 *Chem. Phys.*, 17, 3301–3316, <https://doi.org/10.5194/acp17-3301-2017>, 2017.

762 Li, J., Zhang, Y.L., Cao, F., Zhang, W., Fan, M., Lee, X., and Michalski, G.: Stable sulfur
763 isotopes revealed a major role of transition-metal ion-catalyzed SO₂ oxidation in haze episodes,
764 *Environ. Sci. Technol.*, 54, 2626–2634, <https://doi.org/10.1021/acs.est.9b07150>, 2020.

765 Lind, J. A., Lazrus, A. L., and Kok, G. L.: Aqueous phase oxidation of sulfur (IV) by hydrogen
766 peroxide, methylhydroperoxide, and peroxyacetic acid, *J. Geophys. Res. Atmos.*, 92, 4171-4177,
767 1987.

768 Liu, C., Chen, T., Liu, Y., Liu, J., He, H., Zhang, P.: Enhancement of secondary organic aerosol
769 formation and its oxidation state by SO₂ during photooxidation of 2-methoxyphenol, *Atmos.*
770 *Chem. Phys.*, 19, 2687-2700, 2019.

771 Liu, L., Bei, N., Wu, J., Liu, S., Zhou, J., Li, X., Yang, Q., Feng, T., Cao, J., Tie, X. and Li, G.:
772 Effects of stabilized Criegee intermediates (sCIs) on sulfate formation: a sensitivity analysis
773 during summertime in Beijing–Tianjin–Hebei (BTH), China, *Atmos. Chem. Phys.*, 19, 13341-
774 13354, 2019.

775 Liu, T., Clegg, S. L. and Abbatt, J. P. D.: Fast oxidation of sulfur dioxide by hydrogen peroxide
776 in deliquesced aerosol particles, *Proc. Natl. Acad. Sci. U. S. A.*, 117, 1354–1359, 2020.

777 Liu, Y., Liggio, J., Staebler, R., and Li, S. M.: Reactive uptake of ammonia to secondary organic
778 aerosols: kinetics of organonitrogen formation, *Atmos. Chem. Phys.*, 15, 13569–13584, 2015.

779 Maaß, F., Elias, H., and Wannowius, K. J.: Kinetics of the oxidation of hydrogen sulfite by
780 hydrogen peroxide in aqueous solution: ionic strength effects and temperature dependence,
781 *Atmos. Environ.*, 33, 4413-4419, [https://doi.org/10.1016/S1352-2310\(99\)00212-5](https://doi.org/10.1016/S1352-2310(99)00212-5), 1999.

782 Mauldin, R. L., Berndt, T., Sipilä, M., Paasonen, P., Petäjä, T., Kim, S., Kurtén, T., Stratmann,
783 F., Kerminen, V. M., and Kulmala, M.: A new atmospherically relevant oxidant of sulphur
784 dioxide, *Nature*, 488, 193–196, <https://doi.org/10.1038/nature11278>, 2012.

785 Mekic, M., Loisel, G., Zhou, W., Jiang, B., Vione, D., and Gligorovski, S.: Ionic-strength effects
786 on the reactive uptake of ozone on aqueous pyruvic acid: Implications for air–sea ozone
787 deposition, *Environ. Sci. Technol.*, 52, 12306-12315, 10.1021/acs.est.8b03196, 2018.

788 Mekic, M., Zeng, J., Zhou, W., Loisel, G., Jin, B., Li, X., Vione, D., and Gligorovski, S.: Ionic
789 strength effect on photochemistry of fluorene and dimethylsulfoxide at the air–sea interface:
790 Alternative formation pathway of organic sulfur compounds in a marine atmosphere, *ACS Earth*
791 *Space Chem.*, 4, 1029-1038, 10.1021/acsearthspacechem.0c00059, 2020.

792 Mishra, H., Enami, S., Nielsen, R. J., Hoffmann, M. R., Goddard, W. A., and Colussi, A. J.:
793 Anions dramatically enhance proton transfer through aqueous interfaces, *Proc. Natl. Acad. Sci.*
794 *U. S. A.*, 109, 10228-10232, 2012.

795 Newland, M. J., Rickard, A. R., Vereecken, L., Muñoz, A., Ródenas, M., and Bloss, W. J.:
796 Atmospheric isoprene ozonolysis: impacts of stabilised Criegee intermediate reactions with SO₂,
797 H₂O and dimethyl sulfide, *Atmos. Chem. Phys.*, 15, 9521–9536, [https://doi.org/10.5194/acp-15-](https://doi.org/10.5194/acp-15-9521-2015)
798 9521-2015, 2015.

799 Ng, N., Kroll, J., Chan, A., Chhabra, P., Flagan, R., and Seinfeld, J.: Secondary organic aerosol
800 formation from m-xylene, toluene, and benzene, *Atmos. Chem. Phys.*, 7, 3909–3922,
801 <http://www.atmos-chem-phys.net/7/3909/2007/>, 2007.

802 Ng, N. L., Kwan, A. J., Surratt, J. D., Chan, A. W. H., Chhabra, P. S., Sorooshian, A., Pye, H. O.
803 T., Crouse, J. D., Wennberg, P. O., Flagan, R. C., and Seinfeld, J. H.: Secondary organic
804 aerosol (SOA) formation from reaction of isoprene with nitrate radicals (NO₃), *Atmos. Chem.*
805 *Phys.*, 8, 4117–4140, <http://www.atmos-chem-phys.net/8/4117/2008/>, 2008.

806 Nguyen, T. B., Tyndall, G. S., Crouse, J. D., Teng, A. P., Bates, K. H., Schwantes, R. H.,
807 Coggon, M. M., Zhang, L., Feiner, P., Miller, D. O., Skog, K. M., Rivera-Rios, J. C., Dorris, M.,
808 Olson, K. F., Koss, A., Wild, R. J., Brown, S. S., Goldstein, A. H., de Gouw, J. A., Brune,
809 W. H., Keutsch, F. N., Seinfeld, J. H., and Wennberg, P. O.: Atmospheric fates of Criegee
810 intermediates in the ozonolysis of isoprene, *Phys. Chem. Chem. Phys.*, 18, 10 241–10 254,
811 <https://doi.org/10.1039/C6CP00053C>, <http://dx.doi.org/10.1039/C6CP00053C>, 2016.

812 O'Brien, R. E., Wang, B., Kelly, S. T., Lundt, N., You, Y., Bertram, A. K., Leone, S. R., Laskin,
813 A., and Gilles, M. K.: Liquid–liquid phase separation in aerosol particles: Imaging at the
814 nanometer scale, *Environ. Sci. Technol.*, 49, 4995-5002, [10.1021/acs.est.5b00062](https://doi.org/10.1021/acs.est.5b00062), 2015.

815 Pankow, J. F. and Asher, W. E.: SIMPOL.1: a simple group contribution method for predicting
816 vapor pressures and enthalpies of vaporization of multifunctional organic compounds, *Atmos.*
817 *Chem. Phys.*, 8, 2773–2796, <http://www.atmos-chem-phys.net/8/2773/2008/>, 2008.

818 Qiu, J., Liang, Z., Tonokura, K., Colussi, A. J., and Enami, S.: Stability of monoterpene-derived
819 α -hydroxyalkyl-hydroperoxides in aqueous organic media – relevance to the fate of
820 hydroperoxides in aerosol particle phases, *Environ. Sci. Technol.*, [10.1021/acs.est.9b07497](https://doi.org/10.1021/acs.est.9b07497),
821 2020.

822 Rodríguez-Sevilla, J., Álvarez, M., Limiñana, G., Díaz, M. C.: Dilute SO₂ absorption equilibria
823 in aqueous HCl and NaCl solutions at 298.15 K, *J. Chem. Eng. Data*, 47, 1339-1345, 2002.

824 Ruiz-Lopez, M.F., Francisco, J.S., Martins-Costa, M.T. and Anglada, J.M.: Molecular reactions
825 at aqueous interfaces. *Nat. Rev. Chem.*, 1-17, 2020.

826 Seinfeld, J. H., and Pandis, S. N.: Atmospheric chemistry and physics: from air pollution to
827 climate change, John Wiley & Sons, 2012.

828 Sha, T., Ma, X., Jia, H., Tian, R., Chang, Y., Cao, F., and Zhang, Y.: Aerosol chemical
829 component: Simulations with WRF-Chem and comparison with observations in Nanjing, *Atmos.*
830 *Environ.*, 218, 116982, <https://doi.org/10.1016/j.atmosenv.2019.116982>, 2019.

831 Shang, J., Li, J., Zhu, T.: Heterogeneous reaction of SO₂ on TiO₂ particles. *Sci. China Chem.*, 53,
832 2637–2643, 2010.

833 Shi, G., Xu, J., Peng, X., Xiao, Z., Chen, K., Tian, Y., Guan, X., Feng, Y., Yu, H., Nenes, A.,
834 and Russell, A. G.: pH of aerosols in a polluted atmosphere: Source contributions to highly
835 acidic aerosol, *Environ. Sci. Technol.*, 51, 4289-4296, [10.1021/acs.est.6b05736](https://doi.org/10.1021/acs.est.6b05736), 2017.

836 Shi, Q., Davidovits, P., Jayne, J. T., Worsnop, D. R., and Kolb, C. E.: Uptake of gas-phase
837 ammonia. 1. Uptake by aqueous surfaces as a function of pH, *J. Phys. Chem. A*, 103, 8812-8823,
838 [10.1021/jp991696p](https://doi.org/10.1021/jp991696p), 1999.

839 Song, M., Marcolli, C., Krieger, U. K., Zuend, A., and Peter, T.: Liquid-liquid phase separation
840 in aerosol particles: dependence on O:C, organic functionalities, and compositional complexity,
841 *Geophys. Res. Lett.*, 39, L19801, [doi:10.1029/2012GL052807](https://doi.org/10.1029/2012GL052807), 2012.

842 Song, S., Gao, M., Xu, W., Shao, J., Shi, G., Wang, S., Wang, Y., Sun, Y., and McElroy, M. B.:
843 Fine-particle pH for Beijing winter haze as inferred from different thermodynamic equilibrium
844 models, *Atmos. Chem. Phys.*, 18, 7423-7438, <https://doi.org/10.5194/acp-18-7423-2018>, 2018.

845 Song, S., Gao, M., Xu, W., Sun, Y., Worsnop, D. R., Jayne, J. T., Zhang, Y., Zhu, L., Li, M.,
846 Zhou, Z., Cheng, C., Lv, Y., Wang, Y., Peng, W., Xu, X., Lin, N., Wang, Y., Wang, S., Munger,
847 J. W., Jacob, D. J., and McElroy, M. B.: Possible heterogeneous chemistry of hydroxy
848 methanesulfonate (HMS) in northern China winter haze, *Atmos. Chem. Phys.*, 19, 1357-1371,
849 <https://doi.org/10.5194/acp-19-1357-2019>, 2019.

850 Su, H., Cheng, Y., and Pöschl, U.: New multiphase chemical processes influencing atmospheric
851 aerosols, air quality, and climate in the anthropocene, *Accounts Chem. Res.*, 53, 2034-2043,
852 <https://doi.org/10.1021/acs.accounts.0c00246>, 2020.

853 Sun, Y., Wang, Z., Fu, P., Jiang, Q., Yang, T., Li, J., and Ge, X.: The impact of relative humidity
854 on aerosol composition and evolution processes during wintertime in Beijing, China, *Atmos.*
855 *Environ.*, 77, 927-934, 2013.

856 Surratt, J. D., Murphy, S. M., Kroll, J. H., Ng, N. L., Hildebrandt, L., Sorooshian, A.,
857 Szmigielski, R., Vermeylen, R., Maenhaut, W., and Claeys, M.: Chemical composition of
858 secondary organic aerosol formed from the photooxidation of isoprene, *J. Phys. Chem. A*, 110,
859 9665-9690, 2006.

860 Thornton, J. A., Braban, C. F., and Abbatt, J. P. D.: N₂O₅ hydrolysis on sub-micron organic
861 aerosols: the effect of relative humidity, particle phase, and particle size, *Phys. Chem. Chem*
862 *Phys.*, 5, 4593-4603, <https://doi.org/10.1039/B307498F>, 2003.

863 Tie, X., Brasseur, G., Emmons, L., Horowitz, I., and Kinnison, D.: Effects of aerosols on
864 tropospheric oxidants: a global model study, *J. Geophys. Res. Atmos.*, 106, 22931-22964, 2001.

865 Tong, H., Arangio, A. M., Lakey, P. S. J., Berkemeier, T., Liu, F., Kampf, C. J., Brune, W. H.,
866 Pöschl, U., and Shiraiwa, M.: Hydroxyl radicals from secondary organic aerosol decomposition
867 in water, *Atmos. Chem. Phys.*, 16, 1761-1771, [doi:10.5194/acp-16-1761-2016](https://doi.org/10.5194/acp-16-1761-2016), 2016.

868 Usher, C. R., Al-Hosney, H., Carlos-Cuellar, S., and Grassian, V. H.: A laboratory study of the
869 heterogeneous uptake and oxidation of sulfur dioxide on mineral dust particles, *J. Geophys. Res.*,
870 107, 4713, [doi:10.1029/2002JD002051](https://doi.org/10.1029/2002JD002051), 2002.

871 Varutbangkul, V., Brechtel, F. J., Bahreini, R., Ng, N. L., Keywood, M. D., Kroll, J. H., Flagan,
872 R. C., Seinfeld, J. H., Lee, A., and Goldstein, A. H.: Hygroscopicity of secondary organic
873 aerosols formed by oxidation of cycloalkenes, monoterpenes, sesquiterpenes, and related

874 compounds, *Atmos. Chem. Phys.*, 6, 2367–2388, <http://www.atmos-chem-phys.net/6/23>
875 67/2006/, 2006.

876 Veghte, D. P., Altaf, M. B., and Freedman, M. A.: Size dependence of the structure of organic
877 aerosol, *J. Am. Chem. Soc.*, 135, 16046–16049, 2013.

878 Wang, G., Zhang, R., Gomez, M. E., Yang, L., Zamora, M. L., Hu, M., Lin, Y., Peng, J., Guo, S.,
879 and Meng, J.: Persistent sulfate formation from London Fog to Chinese haze, *Proc. Natl. Acad.*
880 *Sci. U. S. A.*, 113, 13630-13635, 2016.

881 Wang, S., Ye, J., Soong, R., Wu, B., Yu, L., Simpson, A. J., and Chan, A. W. H.: Relationship
882 between chemical composition and oxidative potential of secondary organic aerosol from
883 polycyclic aromatic hydrocarbons, *Atmos. Chem. Phys.*, 18, 3987-4003, 2018.

884 Wang, S., Zhou, S., Tao, Y., Tsui, W. G., Ye, J., Yu, J. Z., Murphy, J. G., McNeill, V. F.,
885 Abbatt, J. P. D., and Chan, A. W. H.: Organic peroxides and sulfur dioxide in aerosol: Source of
886 particulate sulfate, *Environ. Sci. Technol.*, 53, 10695-10704, [10.1021/acs.est.9b02591](https://doi.org/10.1021/acs.est.9b02591), 2019.

887 Wang, X.; Gemayel, R.; Hayeck, N.; Perrier, S.; Charbonnel, N.; Xu, C.; Chen, H.; Zhu, C.;
888 Zhang, L.; Wang, L.; Nizkorodov, S. A.; Wang, X.; Wang, Z.; Wang, T.; Mellouki, A.; Riva, M.;
889 Chen, J.; George, C. Atmospheric photosensitization: A new pathway for sulfate formation,
890 *Environ. Sci. Technol.*, 54, 3114-3120, 2020.

891 Wang, Y., Zhang, Q., Jiang, J., Zhou, W., Wang, B., He, K., Duan, F., Zhang, Q., Philip, S., and
892 Xie, Y.: Enhanced sulfate formation during China's severe winter haze episode in January 2013
893 missing from current models, *J. Geophys. Res. Atmos.*, 119, 10425–10440, 2014.

894 Wei, H., Vejerano, E. P., Leng, W., Huang, Q., Willner, M. R., Marr, L. C., and Vikesland, P. J.:
895 Aerosol microdroplets exhibit a stable pH gradient, *Proc. Natl. Acad. Sci. U. S. A.*, 115, 7272,
896 [10.1073/pnas.1720488115](https://doi.org/10.1073/pnas.1720488115), 2018.

897 Xu, L., Guo, H., Boyd, C. M., Klein, M., Bougiatioti, A., Cerully, K. M., Hite, J. R., Isaacman-
898 VanWertz, G., Kreisberg, N. M., and Knote, C.: Effects of anthropogenic emissions on aerosol
899 formation from isoprene and monoterpenes in the southeastern United States, *Proc. Natl. Acad.*
900 *Sci. U. S. A.*, 112, 37-42, 2015.

901 Yang, Y., Wang, H., Smith, S. J., Easter, R., Ma, P.-L., Qian, Y., Yu, H., Li, C., and Rasch, P. J.:
902 Global source attribution of sulfate concentration and direct and indirect radiative forcing,
903 *Atmos. Chem. Phys.*, 17, 8903–8922, <https://doi.org/10.5194/acp17-8903-2017>, 2017.

904 Yao, M., Zhao, Y., Hu, M., Huang, D., Wang, Y. C., Yu, J. Z., and Yan, N.: Multiphase reactions
905 between secondary organic aerosol and sulfur dioxide: kinetics and contributions to sulfate
906 formation and aerosol aging, *Environ. Sci. Tech. Let.* 6, 768-774, 2019.

907 Ye, J., Gordon, C. A., and Chan, A. W. H.: Enhancement in secondary organic aerosol formation
908 in the presence of preexisting organic particle, *Environ. Sci. Technol.*, 50, 3572-3579, 2016.

909 Ye, J., Abbatt, J. P. D., and Chan, A. W. H.: Novel pathway of SO₂ oxidation in the atmosphere:
910 reactions with monoterpene ozonolysis intermediates and secondary organic aerosol, *Atmos.*
911 *Chem. Phys.*, 18, 5549–5565, <https://doi.org/10.5194/acp18-5549-2018>, 2018.

912 Yee, L. D., Isaacman-VanWertz, G., Wernis, R. A., Kreisberg, N. M., Glasius, M., Riva, M.,
913 Surratt, J. D., de Sá, S. S., Martin, S. T., Alexander, M. L., Palm, B. B., Hu, W., Campuzano-
914 Jost, P., Day, D. A., Jimenez, J. L., Liu, Y., Misztal, P. K., Artaxo, P., Viegas, J., Manzi, A., de

915 Souza, R. A. F., Edgerton, E. S., Baumann, K., and Goldstein, A. H.: Natural and
916 anthropogenically influenced isoprene oxidation in southeastern United States and central
917 Amazon, *Environ. Sci. Technol.*, 54, 5980-5991, 10.1021/acs.est.0c00805, 2020.

918 You, Y., Renbaum-Wolff, L., Bertram, A. K.: Liquid-liquid phase separation in particles
919 containing organics mixed with ammonium sulfate, ammonium bisulfate, ammonium nitrate or
920 sodium chloride, *Atmos. Chem. Phys.*, 13, 11723–11734, [https://doi.org/10.5194/acp-13-11723-](https://doi.org/10.5194/acp-13-11723-2013)
921 2013, 2013.

922 You, Y., Smith, M. L., Song, M., Martin, S. T., and Bertram, A. K.: Liquid–liquid phase
923 separation in atmospherically relevant particles consisting of organic species and inorganic salts,
924 *Int. Rev. Phys. Chem.*, 33, 43–77, doi:10.1080/0144235X.2014.890786, 2014.

925 Zhang, S., Xing, J., Sarwar, G., Ge, Y., He, H., Duan, F., Zhao, Y., He, K., Zhu, L. and Chu, B.:
926 Parameterization of heterogeneous reaction of SO₂ to sulfate on dust with coexistence of NH₃
927 and NO₂ under different humidity conditions, *Atmos. Environ.*, 208, 133-140, 2019.

928 Zhao, Y., Liu, Y., Ma, J., Ma, Q., and He, H.: Heterogeneous reaction of SO₂ with soot: The
929 roles of relative humidity and surface composition of soot in surface sulfate formation, *Atmos.*
930 *Environ.*, 152, 465-476, 2017.

931 Zheng, B., Zhang, Q., Zhang, Y., He, K. B., Wang, K., Zheng, G. J., Duan, F. K., Ma, Y. L., and
932 Kimoto, T.: Heterogeneous chemistry: a mechanism missing in current models to explain
933 secondary inorganic aerosol formation during the January 2013 haze episode in North China,
934 *Atmos. Chem. Phys.*, 15, 2031–2049, doi:10.5194/acp-15-2031-2015, 2015.

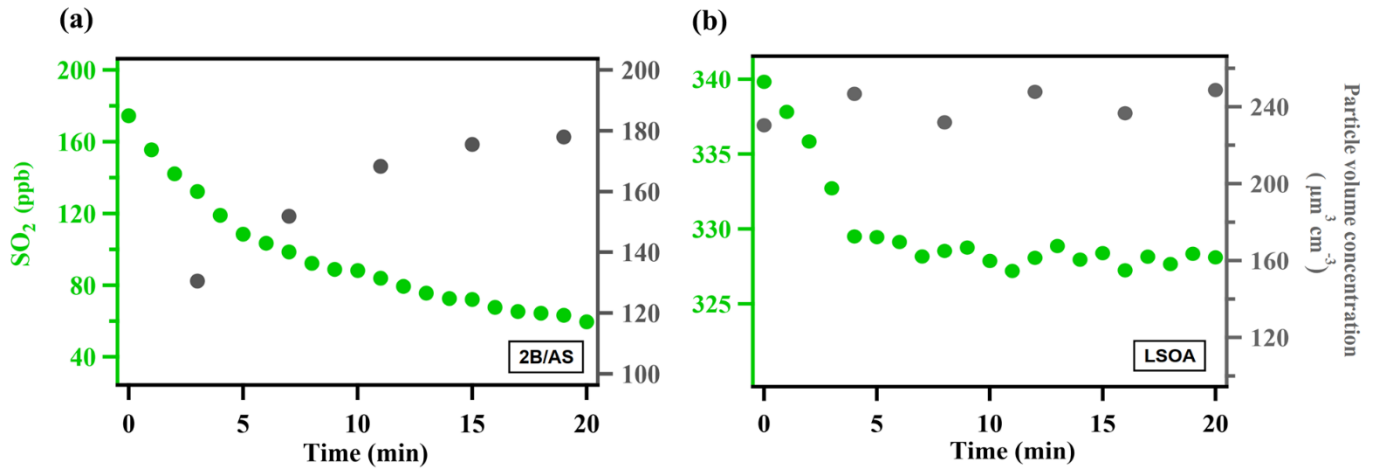
935 Zheng, G. J., Duan, F. K., Su, H., Ma, Y. L., Cheng, Y., Zheng, B., Zhang, Q., Huang, T.,
936 Kimoto, T., Chang, D., Pöschl, U., Cheng, Y. F., and He, K. B.: Exploring the severe winter haze
937 in Beijing: the impact of synoptic weather, regional transport and heterogeneous reactions,
938 *Atmos. Chem. Phys.*, 15, 2969–2983, doi:10.5194/acp-15-2969-2015, 2015.

939 Zheng, G., Su, H., Wang, S., Andreae, M. O., Pöschl, U., and Cheng, Y.: Multiphase buffer
940 theory explains contrasts in atmospheric aerosol acidity, *Science*, 369, 1374-1377,
941 10.1126/science.aba3719, 2020.

942

943

944



945

946 **Figure 1.** Typical evolution of the species monitored during γ_{SO_2} measurement for (a)
 947 ammonium sulfate mixed with 2-butanone organic peroxide (2B/AS, Expt. 16) and (b) limonene
 948 SOA (LSOA, Expt. 27). Particle volume concentrations measured by SMPS have been corrected
 949 for wall loss assuming a pseudo first-order loss rate (Ye et al., 2016). γ_{SO_2} was calculated for the
 950 initial portion of the decay (first 7 minutes).

951

952

953

954

955

956

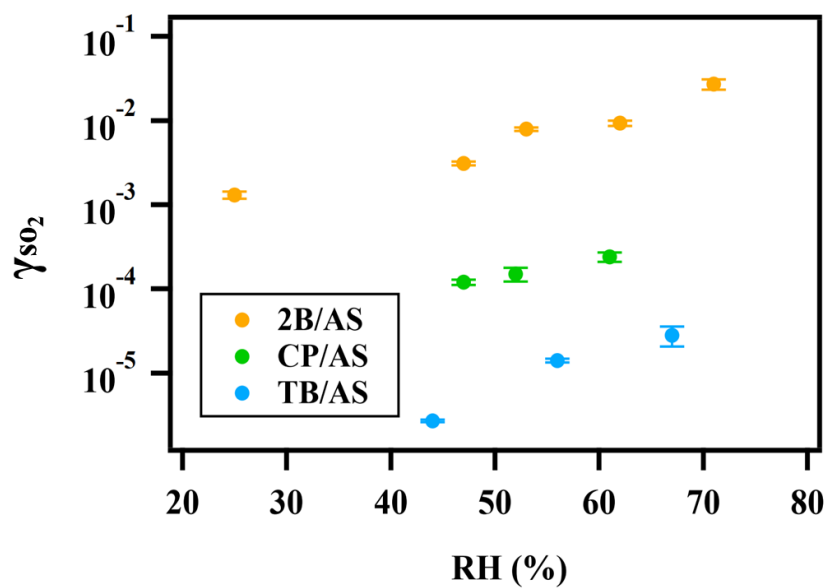
957

958

959

960

961



962

963 **Figure 2.** Exponential relationship between γ_{SO_2} and RH for ammonium sulfate aerosol
 964 containing 2-butanone peroxide (2B), cumene hydroperoxide (CP), tert-butyl hydroperoxide
 965 (TB).

966

967

968

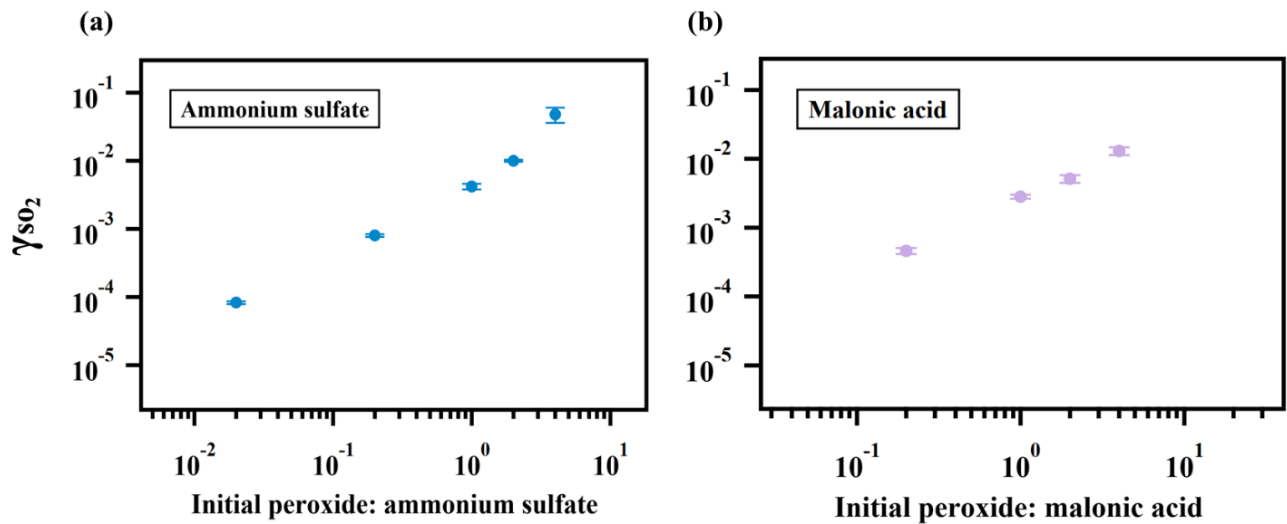
969

970

971

972

973



974

975 **Figure 3.** Relationship between γ_{SO_2} and particulate peroxide content. γ_{SO_2} for ammonium sulfate
 976 (a) and malonic acid aerosol (b) containing different amount of 2-butanone peroxide are shown
 977 here. The observed dependence of γ_{SO_2} on the amount of peroxide injected are linear since the
 978 slopes of the relationship are both nearly 1 in (a) and (b).

979

980

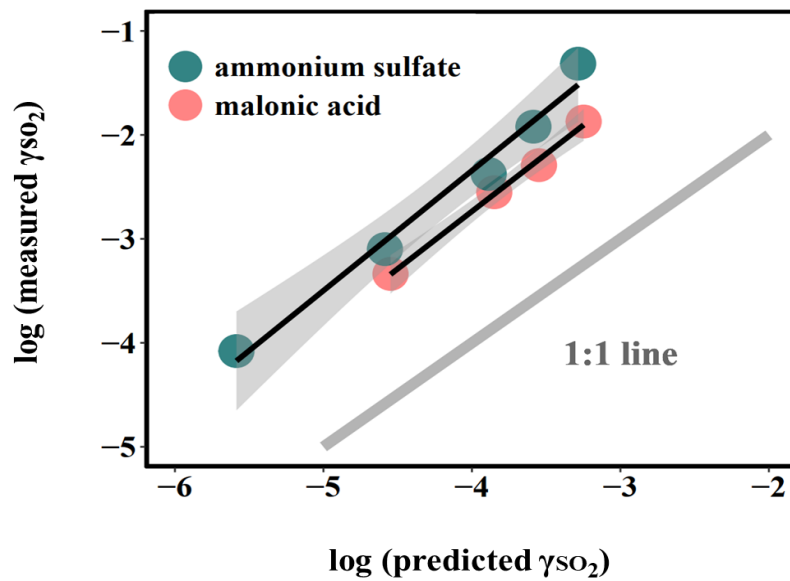
981

982

983

984

985



986

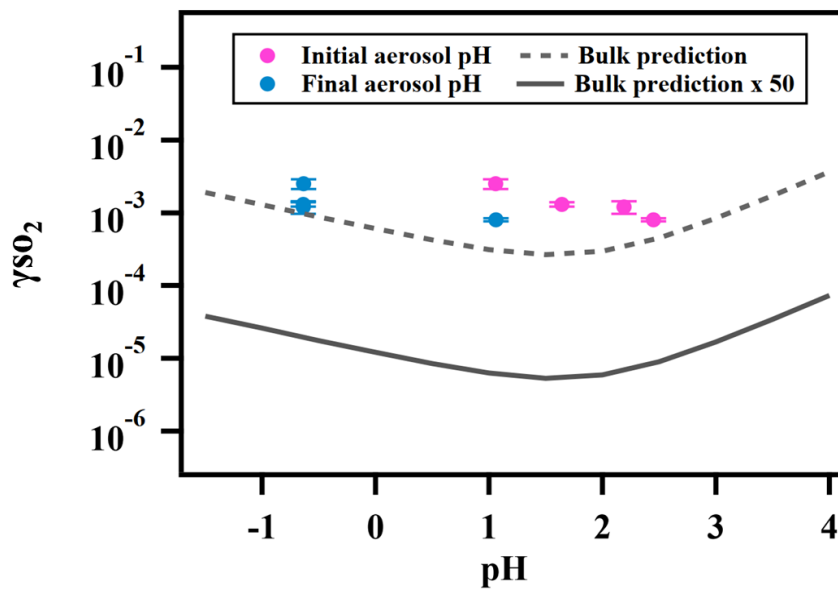
987 **Figure 4.** Relationship between measured γ_{SO_2} and γ_{SO_2} predicted by Eqn. 5. The large deviation
 988 from the 1:1 line, which represents the difference between the measured uptake coefficient and
 989 predicted values based on kinetics in the dilute aqueous phase, indicates that aerosol reactive
 990 uptake is significantly faster than reactions in dilute aqueous phase. This enhancement is likely
 991 driven in part by high ionic strengths, as the difference between measured γ_{SO_2} and predicted γ_{SO_2}
 992 are consistently higher for organic peroxide containing ammonium sulfate (high ionic strength)
 993 than for that mixed with malonic acid (lower ionic strength).

994

995

996

997



998

999 **Figure 5.** Relationship between γ_{SO_2} and aerosol phase pH for ammonium sulfate aerosol
 1000 containing 2-butanone peroxide.

1001

1002

1003

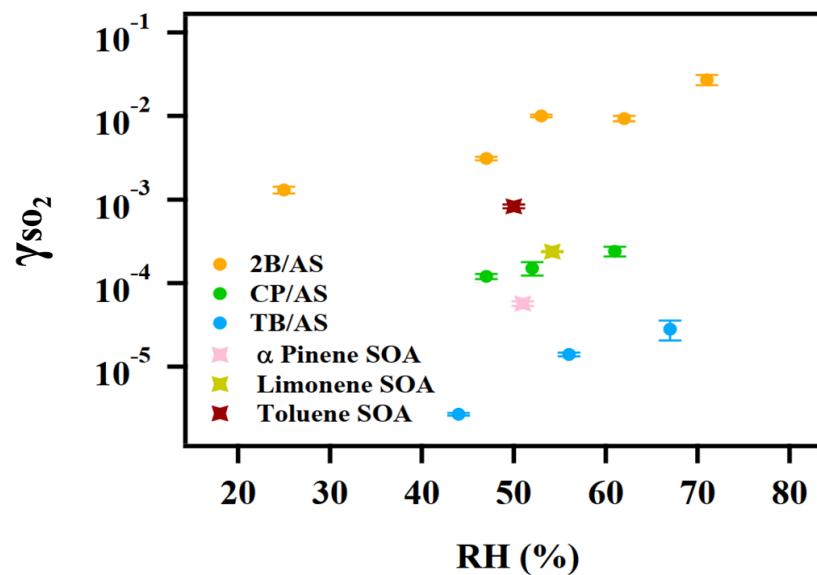
1004

1005

1006

1007

1008



1009

1010 **Figure 6.** γ_{SO_2} measured for different types of organic aerosol. The reactive uptake coefficient of
 1011 SO_2 onto SOA are on the order of 10^{-4} .

1012

1013

1014

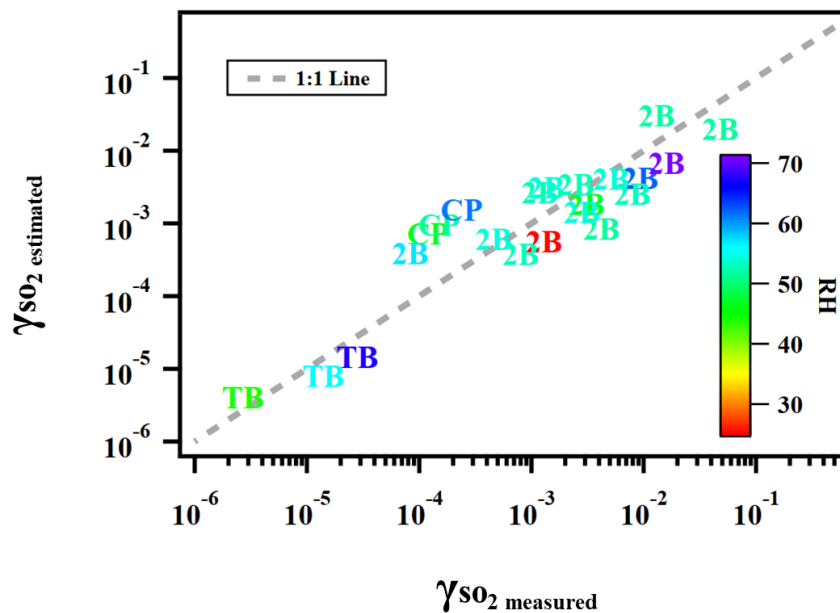
1015

1016

1017

1018

1019



1020

1021 **Figure 7.** Predicted γ_{SO_2} using Equation (13) versus measured γ_{SO_2} for ammonium sulfate or
 1022 malonic acid aerosol containing 2-butanone peroxide (2B), cumene hydroperoxide (CP), tert-
 1023 butyl hydroperoxide (TB) under different experimental conditions.

1024

1025

1026

1027

1028

1029

1030